SHORT TITLE: HopT1-1 directly targets AGO1 to suppress PTI

A bacterial GW-effector directly targets Arabidopsis Argonaute 1 to suppress PAMP-triggered immunity and cause disease

Odon Thiébeauld[1], Magali Charvin[1], Meenu Singla Rastogi[1], Fan Yang[2,3], Dominique Pontier[4], Cécile Pouzet[5], Laure Bapaume[1], Delase Amesefe[1], Guangyong Li[2,3], Laurent Deslandes[6], Thierry Lagrange[4], James R. Alfano[2,3], and Lionel Navarro[1*]

[1] Institut de Biologie de l'Ecole Normale Supérieure (IBENS), Ecole normale supérieure, CNRS, INSERM, PSL Research University, 75005 Paris, France

[2] Department of Plant Pathology, University of Nebraska, Lincoln, NE 68588-0722, USA

[3] Center for Plant Science Innovation, University of Nebraska, Lincoln, NE 68588-0660, USA

[4] Laboratoire Génome et Développement des Plantes, CNRS/Université de Perpignan via Domitia, UMR5096, 66860 Perpignan, France

[5] Plateforme Imagerie-Microscopie, Fédération de Recherche FR3450, CNRS, Castanet-Tolosan, France

[6] LIPM, Université de Toulouse, INRA, CNRS, Castanet-Tolosan, France

O.T. and L.N. conceived and designed the experiments ; O.T. performed most of the experiments, M.S.R., M.C., F.Y., D.P., C.P., L.B., G.L. performed the rest of the experiments; D.A. performed the HopT1-1 sequence alignment ; O.T., M.S.R., L.D., T.L., J.R.A. and L.N. analysed the data ; O.T. and L.N. wrote the article. All the authors edited the article.

* correspondence: lionel.navarro@ens.psl.eu

SUMMARY

***Pseudomonas syringae* (*P. syringae*) type-III effectors were previously found to suppress the Arabidopsis microRNA (miRNA) pathway through unknown mechanisms. Here, we first show that the *P. syringae* HopT1-1 effector promotes pathogenicity by suppressing the Arabidopsis Argonaute 1 (AGO1)-dependent miRNA pathway. We further demonstrate that HopT1-1 physically interacts with Arabidopsis AGO1 through conserved glycine/tryptophan (GW) motifs. Importantly, this AGO-binding platform was found to be essential for the ability of HopT1-1 to suppress both miRNA activity and PAMP-Triggered Immunity (PTI). These results therefore indicate that the RNA silencing suppression activity of HopT1-1 is intimately coupled to its virulence function. Overall, these findings provide the first evidence that a bacterial effector has evolved to directly target an AGO protein to suppress PTI and cause disease.**

INTRODUCTION

Plants and animals have evolved sophisticated inducible immune responses to defend themselves against pathogens. The first layer of the plant immune system relies on the recognition of Pathogen- or Microbe-Associated Molecular Patterns (PAMPs or MAMPs) that are sensed by surface-localized Pattern-Recognition Receptors (PRRs) (Couto and Zipfel, 2016). Classical plant PRRs are composed of receptor-like kinases (RLKs) and receptor-like proteins (RLPs) that are structurally and functionally analogous to animal Toll-Like Receptors (TLRs) (Li *et al*., 2016). The most characterized plant PRRs are the leucine-rich repeat RLKs Flagellin Sensing 2 (FLS2) and EF-Tu Receptor (EFR), which recognize conserved epitopes from

bacterial flagellin or elongation factor Tu, respectively (Gómez-Gómez and Boller, 2000; Zipfel *et al*., 2006). Upon ligand binding, these receptors initiate a complex phosphorylation cascade at the PRR complex that leads to early signaling events, which include production of reactive oxygen species (ROS), activation of mitogen-activated-protein-kinases (MAPKs) and differential expression of thousands of genes (Gómez-Gómez *et al*. 1999; Felix *et al.*, 1999; Zipfel *et al*., 2004; Navarro *et al*., 2004; Zipfel *et al*., 2006; Couto and Zipfel, 2016). Later responses involve biosynthesis of the phytohormone salicylic acid (SA) and cell wall modifications such as callose deposition, which ultimately culminate in PAMP-triggered immunity (PTI) (Hauck *et al*., 2003; Tsuda and Katagiri, 2010). Pathogens secrete virulence determinants, referred to as pathogen effectors, which can suppress PTI to cause disease (Jones and Dangl, 2006). As a counter-counter defense mechanism, plants have evolved disease resistance (R) proteins that can recognize the presence of pathogen effectors. A major class of R proteins is composed of intracellular immune receptors that belong to the nucleotide-binding domain (NBD), leucine-rich repeat (NLR) superfamily, which is also present in animals (Jones *et al*., 2016). After sensing pathogen effectors, plant NLRs induce Effector-triggered immunity (ETI), a potent immune response that significantly overlaps with PTI, although with a stronger amplitude (Tsuda and Katagiri, 2010; Navarro *et al*., 2004). Recently, several endogenous short interfering RNAs (siRNAs) and microRNAs (miRNAs) were found to fine-tune PTI and ETI responses (Staiger *et al*., 2013; Pumplin and Voinnet, 2013), implying a key role of Post-Transcriptional Gene Silencing (PTGS) in the regulation of the plant immune system.

PTGS is an ancestral post-transcriptional gene regulatory process. The core mechanism of PTGS involves the production of double-stranded RNA (dsRNA)

precursors, which are processed by DICER-LIKE (DCL) enzymes into 20-24 bp small RNA duplexes (Bologna and Voinnet, 2014). These small RNA duplexes associate with an Argonaute (AGO) protein, the central component of a multi-protein RNA-induced silencing complex (RISC) (Vaucheret, 2008). The guide small RNA further directs AGO-RISC to sequence complementary mRNA targets to trigger their post-transcriptional gene silencing. In plants, this phenomenon is manifested by endonucleolytic cleavage (so-called 'slicing') and/or translational inhibition of small RNA targets (Llave *et al*., 2002; Rhoades *et al*., 2002; Palatnik *et al*., 2003; Brodersen *et al*., 2008; Chen, 2004; Poulsen *et al*., 2013). *Arabidopsis thaliana* encodes 4 DCLs and 10 AGOs. DCL1 processes miRNA precursors with the help of other factors including the zinc-finger domain-containing protein SERRATE (SE) (Park *et al*., 2002; Finnegan *et al*., 2003; Kurihara and Watanabe, 2004; Lobbes *et al*., 2006). This reaction yields miRNA/miRNA* duplexes, where miRNA is the guide strand and miRNA* is the passenger strand. DCL2, DCL3 and DCL4 process endogenous and viral-derived dsRNAs into siRNA duplexes (Bologna and Voinnet, 2014). A significant proportion of dsRNAs is produced by RNA-dependent RNA polymerases (RDRs) that convert single-stranded RNAs (ssRNAs) into dsRNAs. RDR6, which is one of the six Arabidopsis RDRs, produces dsRNAs from viral transcripts, transposable elements, as well as from endogenous transcripts (Mourrain *et al.*, 2000; Dalmay *et al.*, 2000; Allen *et al.*, 2005; Fei *et al.*, 2013; Nuthikattu *et al.*, 2013). In the latter pathway, the siRNAs are generated from the combined action of primary siRNA/miRNA-directed transcript targeting and of RDR6 activity, which results in the production of dsRNAs that are subsequently processed by DCL4 into 21nt secondary siRNAs, which can be phased and thus referred to as "phasiRNAs" (Allen *et al.*, 2005; Xie *et al.*, 2005; Fei *et al.*, 2013, Arribas-Hernández *et al.*, 2016).

AGO1 is a major PTGS factor, which is loaded with miRNAs, (pha)siRNAs or viral-derived siRNAs and plays an important role in plant development (Bohmert *et al.*, 1998; Fagard *et al.*, 2000), antiviral defense (Morel *et al*., 2002) as well as bacterial PAMP-induced gene induction and callose deposition (Li *et al*., 2010). AGO2 not only plays a critical role in antiviral silencing but is also required for antibacterial resistance mediated by the disease resistance protein RPS2 (Carbonell *et al*., 2012; Harvey *et al*., 2011; Jaubert *et al*., 2011; Zhang *et al*., 2011). AGO4 has also been reported to modulate antiviral silencing as well as antibacterial defense (Agorio and Vera, 2007; Brosseau *et al*., 2016).

Small non-coding RNAs have been implicated in various biological processes and play a key role in controlling plant-pathogen interactions. In the context of plant-viral interactions, viral-derived siRNAs repress translation, replication or accumulation of viral RNAs, thereby inhibiting viral replication (Hamilton and Baulcombe, 1999; Pumplin and Voinnet, 2013; Baulcombe, 2015). In addition, plant miRNAs and siRNAs can modulate resistance against bacterial, fungal and oomycete phytopathogens by targeting either positive or negative regulators of PTI and/or ETI (Weiber *et al*., 2015). This phenomenon has been well characterized in the context of plant-bacterial interactions. As examples, miR393, miR160 and miR167 are PAMP-induced miRNAs that are loaded into Arabidopsis AGO1 to negatively regulate auxin signaling during PTI (Navarro *et al.*, 2006; Fahlgren *et al*., 2007; Li *et al.*, 2010), while miR393b* is enriched in Arabidopsis AGO2 during ETI and targets a negative regulator of defense that acts downstream of RPS2 (Zhang *et al.*, 2011). Furthermore, several endogenous siRNAs were found to be induced in response to a *P. syringae* strain carrying *AvrRpt2* and specifically required for RPS2-mediated

resistance (Katiyar-Agarwal *et al*., 2006; 2007). It has also been reported that filamentous phytopathogens differentially regulate functionally relevant small RNAs during infection. For example, soybean miR393 is induced in response to *Phytophthora sojae* and positively regulates resistance against this oomycete pathogen (Wong *et al*., 2014). Besides their role in fine-tuning PTI and ETI responses, there is also growing evidence that endogenous plant siRNAs and miRNAs can be transferred into oomycetal and fungal cells to trigger PTGS of factors required for the multiplication of these filamentous pathogens (Wang *et al*., 2016; Cai *et al*., 2018; Hou *et al*., 2019).

Given that small non-coding RNAs play a major role in regulating plant immune responses as well as in targeting viral, fungal and oomycetal transcripts, it is not surprising that many pathogens have evolved PTGS suppression mechanisms to cause disease. This phenomenon has been extensively characterized in plant-viral interactions and we know now that most, if not all, plant RNA viruses encode Viral Suppressors of RNA silencing (VSRs) (Pumplin and Voinnet, 2013). These proteins suppress different steps of PTGS and AGO1 has emerged as a critical VSR target (Zhang *et al.,* 2006; Derrien *et al*., 2012; Azevedo *et al*., 2010; Giner *et al*., 2010). Interestingly, RNA silencing suppressors were also reported from bacterial, oomycete and fungal phytopathogens (Navarro *et al*., 2008; Qiao *et al*., 2013, Qiao *et al*., 2015; Hou *et al.*, 2019; Yin *et al.*, 2019). In particular, we found that growth of a type-III secretion defective mutant of *Pto* DC3000 and of non-adapted bacteria was significantly enhanced in Arabidopsis mutants that are impaired in miRNA biogenesis (Navarro *et al*., 2008). These results provide evidence that the Arabidopsis miRNA pathway is essential for basal immunity and suggest that *Pto* DC3000 effectors must

have evolved to suppress this small RNA pathway to cause disease. Accordingly, we have identified a series of Bacterial Suppressors of RNA silencing (BSRs) from this bacterium that inhibit all the steps of the Arabidopsis miRNA pathway (Navarro *et al*., 2008). However, it remains unknown whether such BSRs could directly interact with components of the RNA silencing machinery and alter their activity as part of their virulence functions.

Here, we found that the type-III secreted Hrp outer protein T1-1 (HopT1-1) is a critical virulence determinant of *Pto* DC3000 that promotes pathogenicity by suppressing the AGO1-dependent miRNA pathway. We show that HopT1-1 interacts with Arabidopsis AGO1 through conserved GW motifs, which represent AGO-binding platforms previously found in some metazoan and plant AGO cofactors (Till *et al*., 2007; El-Shami *et al*., 2007; Azevedo *et al*., 2011). We provide further evidence that these AGO-binding platforms are essential for the ability of HopT1-1 to suppress not only miRNA activity but also PTI. These results indicate that the silencing suppression activity of HopT1-1 is coupled to its virulence function and relies, at least in part, on the targeting of Arabidopsis AGO1. This study therefore demonstrates that the bacterial effector HopT1-1 has evolved to directly target AGO1 to suppress PTI and cause disease.

RESULTS

HopT1-1 is a key pathogenicity determinant that promotes growth of *Pto* DC3000 by suppressing the Arabidopsis AGO1-dependent miRNA pathway

HopT1-1 is an experimentally validated type-III secreted protein expressed from the pDC3000A plasmid of *Pto* DC3000 (Guo *et al*., 2005). Although HopT1-1 was previously shown to suppress the transcriptional activation of a PAMP-responsive gene (Li *et al*., 2005), there is so far no experimental evidence indicating a role for this effector in promoting bacterial multiplication *in planta*. To test this possibility, we first generated a *Pto* DC3000 mutant strain deleted of *hopT1-1*, hereafter referred to as *Pto* Δ*hopT1-1*, and assessed the ability of this strain to multiply in leaves of the Arabidopsis Col-0 reference accession. Upon dip-inoculation of wild type (WT) plants, we found that the *Pto* Δ*hopT1-1* mutant strain exhibited at least ~ 10 times lower bacterial titer at 3 days post-inoculation (dpi) compared to the WT *Pto* DC3000 strain (Figures 1 and S1). This result indicates that HopT1-1 is a functionally relevant effector of *Pto* DC3000 that contributes to bacterial growth *in planta*.

HopT1-1 was previously shown to suppress AGO1-mediated miRNA- and siRNA-functions (Navarro *et al*., 2008), but the relevance of this interference in bacterial pathogenesis remains unknown. We took advantage of the *Pto* Δ*hopT1-1* mutant strain and examined whether its growth defect could be potentially rescued in *ago1* mutants. For this purpose, we dip-inoculated the *Pto* Δ*hopT1-1* strain on WT plants and on three hypomorphic *ago1* mutants, namely *ago1-25*, *ago1-26* and *ago1-27* (Morel *et al*., 2002), and subsequently monitored bacterial titers at 3 dpi. We also included in this assay the *ago2-1*, *ago4-2* and *ago4-3* mutants, as *AGO2* and *AGO4* were previously characterized in RPS2-mediated resistance and in antibacterial basal resistance, respectively (Zhang *et al*., 2011; Agorio and Vera, 2007). Importantly, the growth defect of *Pto* Δ*hopT1-1* was fully rescued in all *ago1* allelic mutants (Figures 1A, S1A and S1B), while it remained unaltered in *ago2* and *ago4* mutants (Figures 1B and S1C). To further test whether the phenotype observed in

ago1 mutants was specific to the *Pto* Δ*hopT1-1* mutant strain, and not due to collateral effects caused by *ago1* developmental phenotypes, we repeated this assay with a *Pto* DC3000 mutant deleted of *hopC1* (*Pto* Δ*hopC1*). The latter effector partially contributes to *Pto* DC3000 multiplication in Arabidopsis WT leaves but does not interfere with miRNA action (Figures 1A and S1A; Navarro *et al*., 2008). Importantly, the partial *Pto* Δ*hopC1* growth defect observed in WT plants was not rescued in *ago1-27* plants (Figures 1A and S1A), indicating that the restoration of bacterial growth detected in *ago1* mutants was specific to the *Pto* Δ*hopT1-1* strain. Collectively, these results indicate that *AGO1* is a major genetic target of HopT1-1. They also suggest that AGO1 function(s) must be impaired by HopT1-1 to promote growth of *Pto* DC3000 *in planta*.

Given that AGO1 is required for both miRNA- and siRNA- functions, we next assessed which of the two activities could be genetically targeted by HopT1-1 to promote growth of *Pto* DC3000 *in planta.* We first tested whether the *Pto* Δ*hopT1-1* growth defect could be rescued in *dcl1-11* and *se-1* mutants, which are both impaired in miRNA biogenesis (Lobbes *et al*., 2006; Zhang *et al*. 2008). Similar to the observation made in *ago1* mutant alleles, the *Pto* Δ*hopT1-1* growth defect was fully restored in these mutants (Figures 1C, S1D and S1E). We then repeated the same assay in *suppressor of gene silencing 3* (*sgs3-1*), *rdr1-1 rdr2-1 rdr6-15* triple and *dcl2-1 dcl4-2* double mutants, which are impaired in the biogenesis of endogenous siRNAs and viral-derived siRNAs (Mourrain *et al*., 2000; Dalmay *et al*., 2000; Xie *et al*., 2004; Deleris *et al*., 2006; Diaz-Pendon *et al*., 2007; Donaire *et al*., 2008), but did not find any growth restoration of the *Pto* Δ*hopT1-1* strain in these siRNA-defective mutants (Figures 1D, S1F and S1G). Altogether, these results indicate that HopT1-1-

triggered suppression of AGO1-mediated miRNA function is critical to promote growth of *Pto* DC3000 *in planta*.

HopT1-1 physically interacts with Arabidopsis AGO1 through two conserved GW motifs

The above genetic data suggested that HopT1-1 could interact with Arabidopsis AGO1 to alter its miRNA-related function. The AGO-binding function of GW/WG platforms, present in some endogenous silencing factors as well as in some VSRs (El-Shami *et al.*, 2007; Azevedo *et al*., 2011; Azevedo *et al*., 2010; Giner *et al*., 2010; Garcia *et al.*, 2012; Aqil *et al*., 2013; Karran and Sansfaçon, 2014) prompted us to examine the protein sequence of HopT1-1 for the presence of such motifs. We found that there are three GW repeats at positions 80, 113 and 182, which are referred to here as GW1, GW2 and GW3, respectively (Figure 2A). Furthermore, these GW motifs were found conserved in a putative HopT1-1 ortholog derived from the phylogenetically divergent marine bacterium *Marinomonas mediterranea* (Figure 2A), suggesting that they might be functionally relevant. To test this hypothesis, we generated tryptophan to phenylalanine substitutions (GW>GF) in each tryptophan residue of the GW motifs. It is noteworthy that these point mutations do not alter the stability of HopT1-1 when expressed *in planta* (Figure S2A). We further analyzed the ability of HopT1-1 WT and of the triple GW>GF mutant version, referred to as HopT1-1m3, to bind to AGO1 *in planta*. To gain insight into this possibility, we first conducted bimolecular fluorescence complementation (BiFC) assays upon Agrobacterium-mediated transient transformation of *N. benthamiana* leaves with constructs carrying the N-terminal fragment of the Yellow Fluorescence Protein (YFP) translationally fused to Arabidopsis AGO1 and the C-terminal fragment of the YFP fused with

HopT1-1 or HopT1-1m3. In these experiments, we also used split-YFP fusions of HopC1 and of the silencing factor Silencing Defective 3 (SDE3) as negative controls. All these constructs were under the control of the moderately active *ubiquitin-10* promoter, which is suitable for transient expression of fluorescent-tagged proteins in *N. benthamiana* (Grefen *et al*., 2010). Confocal imaging revealed a clear fluorescence emission in epidermal cells co-expressing CYFP-HopT1-1/NYFP-AGO1 fusions, which was significantly different from the baseline fluorescent signal observed in cells co-expressing CYFP-HopC1/NYFP-AGO1 or CYFP-HopT1-1/NYFP-SDE3 fusions (Figure 2B). These observations indicate that HopT1-1 is found in a close proximity to AGO1 *in planta*, which is not the case of SDE3 nor of HopC1, a *Pto* DC3000 effector that cannot suppress miRNA activity nor target AGO1 genetically (Figures 1A and S1A; Navarro *et al*., 2008). Importantly, we did not find any fluorescence emission upon co-expression of CYFP-HopT1-1m3/NYFP-AGO1 fusions (Figure 2B), indicating that the GW motifs of HopT1-1 are essential to ensure its close proximity to AGO1 in plant cells.

To further test whether HopT1-1 could physically interact with AGO1 *in planta*, we next decided to use a non-invasive fluorescence imaging approach by conducting Föster resonance energy transfer-fluorescence lifetime imaging microscopy (FRET-FLIM) analyses after co-expressing a cyan fluorescent protein (CFP)-AGO1 (*35S$_{pro}$:CFP-AGO1*) with either *35S$_{pro}$:HopT1-1-YFP* or *35S$_{pro}$:HopT1-1m3-YFP* constructs in *N. benthamiana* leaves. By doing so, we found a significant reduction in the average CFP lifetime of the donor CFP-AGO1 molecules in plant cells co-expressing CFP-AGO1/HopT1-1-YFP compared with those co-expressing CFP-AGO1/HopT1-1-HA or expressing CFP-AGO1 alone (Figure 2C, Figure S2B, S2C), further supporting a physical interaction between HopT1-1 and AGO1 *in planta*.

Importantly, this protein-protein interaction was fully dependent on the GW motifs of HopT1-1 because we did not detect any FRET in plant cells co-expressing CFP-AGO1 and HopT1-1m3-YFP (Figure 2C, Figure S2B). Altogether, these data provide evidence that HopT1-1 interacts with AGO1 in plant cells and that this process is fully dependent on its GW-dependent AGO-binding platform.

To further confirm the above results *in vitro* and get insights into the contribution of each GW motif in HopT1-1-AGO1 interaction, we first attempted to produce recombinant GST-HopT1-1 in *Escherichia coli*. However, GST-HopT1-1 was mainly present in the insoluble protein fraction, preventing further analysis with the full-length protein (data not shown). To circumvent this problem, we next decided to chemically synthesize biotinylated peptides containing each GW motif surrounded by native amino acid residues. As negative controls, we synthesized mutated peptides with phenylalanine substitutions in the tryptophan of each GW motif (Figure 2D). Equimolar amount of the peptides was bound to streptavidin columns (Figure S3), and then incubated with inflorescence extracts from FLAG-AGO1 transgenic plants. After washing, eluted streptavidin-bound proteins were analyzed by Western blot using anti-FLAG antibody. Using this approach, we observed that the HopT1-1 GW2 and GW3 peptides, which exhibit the highest score for GW motif prediction (Figure 2A, Zielezinski and Karlowski, 2015), were both bound to FLAG-AGO1 protein, while the HopT1-1 GW1 peptide was not (Figure 2D). Furthermore, binding to FLAG-AGO1 was partially or completely lost upon incubation of inflorescence extracts from FLAG-AGO1 plants with the mutated HopT1-1 GF2 and GF3 peptides, respectively (Figure 2D). These additional *in vitro* results support our BiFC and FRET-FLIM data and further indicate that HopT1-1 physically interacts with Arabidopsis AGO1 through, at least in part, the two conserved GW2 and GW3 motifs.

HopT1-1 suppresses AGO1-mediated miRNA activity in a GW-dependent manner

To further test the requirement of the GW motifs of HopT1-1 in RNA silencing suppression, we have analyzed the ability of HopT1-1 and HopT1-1m3 to suppress AGO1 miRNA activity *in vivo*. For this end, we transformed the Arabidopsis Col-0 accession (WT) with either a *35S$_{pro}$:HopT1-1* or a *35S$_{pro}$:HopT1-1m3* construct and further monitored the accumulation of AGO1-dependent miRNA targets in individual primary transformants (n = 12 or 13 individuals) expressing comparable levels of *HopT1-1* and of *HopT1-1m3* transcripts (Figures 3A, S4A). Real-time quantitative PCR (RT-qPCR) analyses revealed a significant enhanced mRNA accumulation of the miRNA targets *SPL10* (miR156), *MYB33* (miR159), *MYB65* (miR159), *ARF10* (miR160), *ARF17* (miR160), *PHB* (miR166), *ARF6* (miR167), *ARF8* (miR167) and *HAP2B* (miR169) in HopT1-1 lines compared to Col-0 control plants (Figures 3B, S4B). Derepression of *SPL10* (miR156), *ARF17* (miR160), *PHB* (miR166), *ARF6* (miR167), *ARF8* (miR167) and *HAP2B* (miR169) was also detected in the hypomorphic *ago1-27* mutant (Figure 3B), which served as a positive control in these RT-qPCR experiments. In addition, the levels of *AGO1*, *AGO2* and *DCL1* transcripts, which are controlled by miR168, miR403 and miR162/838, respectively (Xie *et al.*, 2003; Vaucheret *et al.*, 2004; Allen *et al.*, 2005; Rajagopalan *et al.*, 2006); were more elevated in HopT1-1 lines compared to Col-0 plants (Figures 3C, S4C), and this effect was associated with an enhanced accumulation of cognate proteins in these transgenic lines as revealed by Western blot analyses (Figures 3D, S4D). An enhanced accumulation of *AGO1* and *AGO2* mRNAs, as well as of AGO2 and DCL1 proteins, was also observed in *ago1-27* compared to WT plants (Figure 3C, 3D).

However, we found that AGO1 protein levels remained low in *ago1-27* plants (Figure 3D), which is probably due to the remaining negative regulation exerted by AGO10 over AGO1 protein accumulation in this *ago1* hypomorphic mutant (Mallory *et al.*, 2009). Furthermore, mRNA and protein levels of AGO4, which is not targeted by small RNAs, were unchanged in HopT1-1 transgenic lines and in *ago1-27* plants compared to WT plants (Figure 3C, 3D), indicating a specific effect of HopT1-1 over miRNA targets. In addition, we found that all the above miRNA targets remained fully silenced in HopT1-1m3 plants (Figure 3B-D, S4B-D), implying a key role of the AGO-binding platform of HopT1-1 in their derepression. Collectively, these data provide evidence that HopT1-1 suppresses AGO1-dependent miRNA activity in a GW-dependent manner.

HopT1-1 triggers a moderate decrease in the accumulation of conserved miRNAs, with no, or negligible, effect on the accumulation of pri-miRNAs

We next assessed whether the silencing suppression activity of HopT1-1 could be due to an alteration in miRNA biogenesis and/or stability. For this purpose, we first performed low molecular weight Northern analyses from pooled leaf samples of *35S$_{pro}$:HopT1-1* and *35S$_{pro}$:HopT1-1m3* primary transformants. Using this assay, we found a moderate decrease in the accumulation of a subset of conserved Arabidopsis miRNAs in *35S$_{pro}$:HopT1-1* primary transformants compared to Col-0 or *35S$_{pro}$:HopT1-1m3* transgenic plants (Figures 4A, S5A). More specifically, an average of ~2-fold decrease in the levels of miR156, miR159, miR166 and miR167 was observed in *35S$_{pro}$:HopT1-1 versus 35S$_{pro}$:HopT1-1m3* primary transformants, while this effect was not consistently detected among biological replicates for miR168 (Figure 4A). We also noticed that HopT1-1 triggers the additional production of longer

miR166 species that are ~24 nt in length, a phenomenon that was not observed in the presence of HopT1-1m3 (Figures 4A, S5A). To determine whether the above molecular effects could be due to an interference of HopT1-1 with the processing of pri-miRNAs, we further monitored the accumulation of primary miRNA transcripts in the primary transformants by RT-qPCR analyses. We found that the levels of *pri-miR156a*, *pri-miR166a* and *pri-miR167a* were either unchanged or barely affected in HopT1-1 transgenic lines (Figures 4B, S5B), indicating that HopT1-1 does not alter the processing of these pri-miRNAs. Nonetheless, a mild increase in the accumulation of *pri-miR159b* and *pri-miR168a* was specifically detected in HopT1-1 primary transformants (Figures 4B, S5B), although this effect was much weaker than the one observed in the miRNA biogenesis-defective *dcl1-11* and *se-1* mutants (Figures 4B, S5B; Zhang *et al.*, 2008; Yang *et al.*, 2006; Lobbes *et al.*, 2006). Altogether, these data indicate that the AGO-binding platform of HopT1-1 triggers a moderate decrease in the accumulation of a subset of conserved miRNAs, which is unlikely caused by an impairment of the processing of cognate pri-miRNAs. They also suggest that the BSR activity of HopT1-1 mostly interferes with the AGO1-miRISC activity rather than with the biogenesis or stability of endogenous miRNAs.

HopT1-1 suppresses PTI responses in a GW-dependent manner and its presence mimics the impaired PTI responses observed in *ago1* mutants

Given that the majority of *Pto* DC3000 effectors promotes pathogenicity by dampening plant immune responses (Block and Alfano, 2011), we further investigated the ability of HopT1-1 to suppress PTI. Furthermore, the fact that HopT1-1 promotes pathogenicity through the targeting of AGO1 (Figures 1A, S1A and S1B) prompted us to assess the functional relevance of its AGO-binding platform

in this process. To address these questions, we decided to use the EtHAn system, a recombinant *P. fluorescens* strain that triggers classical PTI responses and that expresses a functional type-III secretion system, allowing the delivery of individual bacterial effectors in host cells (Thomas *et al*., 2009). It is noteworthy that this experimental system has been successfully used to characterize the PTI suppression activities of individual *Pto* DC3000 effectors during infection (Thomas *et al*., 2009). Col-0 WT plants were infiltrated with EtHAn alone or with EtHAn strains expressing either HopT1-1 (EtHAn (HopT1-1)) or HopT1-1m3 (EtHAn (HopT1-1m3)) and the production of the reactive oxygen intermediate hydrogen peroxide (H_2O_2) was monitored at 24 hours post-inoculation by DAB staining (Figure 5A). While the EtHAn strain induced strong production of H_2O_2 in WT plants, particularly within and around leaf vasculature, this phenotype was significantly reduced upon delivery of HopT1-1 (Figure 5A). This result indicates that HopT1-1 can inhibit PAMP-triggered production of H_2O_2 in a physiological context of bacterial infection. By contrast, this PTI suppression effect was almost fully abolished upon delivery of the HopT1-1m3 mutant version (Figure 5A), supporting a critical role for the GW motifs of HopT1-1 in this process. In addition, we exploited the EtHAn system to monitor the impact that HopT1-1, and its HopT1-1m3 mutant derivative, could have on bacterial-triggered deposition of callose, a late PTI response that plays a critical role in the establishment of basal immunity (Hauck *et al*., 2003). Interestingly, we found a ~ 45% decrease in the number of callose deposits in response to EtHAn (HopT1-1) as compared to the EtHAn control, while this PTI suppression effect was not observed upon inoculation of the EtHAn (HopT1-1m3) strain (Figure 5B). Taken together, these data indicate that HopT1-1 can suppress two well-established PTI responses during

bacterial infection. They also provide evidence that the RNA silencing suppression activity of HopT1-1 is directly coupled with its ability to dampen PTI in Arabidopsis.

Given that AGO1 is a critical target of HopT1-1 (Figures 1 and 2), the above findings suggested a major role for AGO1 in orchestrating PTI. To test this possibility, we first monitored flg22-triggered oxidative burst in the *ago1-25*, *ago1-26* and *ago1-27* hypomorphic mutant alleles. Importantly, all these *ago1* mutants displayed a compromised flg22-induced ROS production as compared to WT-elicited plants (Figure 5C). A significantly impaired flg22-induced ROS production was also detected in the miRNA biogenesis defective mutants *dcl1-11* and *se-1* as compared to WT plants (Figure 5D), indicating that the Arabidopsis miRNA pathway positively regulates this early PTI response. Hydrogen peroxide production and callose deposition were also reduced in *ago1-27* mutants *versus* WT plants challenged with the EtHAn strain (Figures 5E and 5F), although a milder effect was observed in this mutant background as compared to the effect detected in WT leaves challenged with the EtHAn (HopT1-1) strain (Figures 5A and 5B). These results support a role for AGO1 in PAMP-induced callose deposition, as previously reported during flg22 elicitation (Li *et al*., 2010). In addition, they provide evidence that AGO1 plays a central role in the production of ROS during bacterial elicitation. Altogether, these data suggest that the ability of HopT1-1 to suppress both PAMP-triggered ROS production and callose deposition involves, at least in part, an inhibitory effect of AGO1 activity.

DISCUSSION

In the present study, we have demonstrated a key role for the Arabidopsis miRNA pathway in PAMP-induced ROS production, a well-characterized PTI response that

occurs within minutes of PAMP detection and that plays a crucial role in antibacterial defense (Couto and Zipfel, 2016; Torres *et al*., 2006). We have shown that the Arabidopsis miRNA factors DCL1, SE and AGO1 are all required for flg22-induced oxidative burst (Figure 5). Furthermore, we found that the EtHAn strain triggers an intense accumulation of H_2O_2 within and around Arabidopsis leaf vasculature, a phenotype that was partially impaired in the hypomorphic *ago1-27* mutant (Figure 5). Such AGO1-dependent regulatory process might ensure the formation of an immune cell layer adjacent to the vasculature to limit bacterial spreading from xylem vessels to mesophyll cells and *vice versa*. In addition, this phenomenon might result in an enhanced accumulation of H_2O_2 in xylem vessels, thereby potentially reducing bacterial survival through the well-characterized bactericidal function of this reactive oxygen intermediate (Hong *et al*., 2013). Such an antibacterial activity would notably be relevant to control *Pto* DC3000 pathogenesis because this bacterium was previously shown to propagate through xylem vessels in both Arabidopsis and *N. benthamiana* (Yu *et al*., 2013; Misas-Villamil *et al*., 2011). Although the detailed mechanisms by which the Arabidopsis miRNA pathway orchestrates ROS production, and more generally PTI, remain to be established, we propose that the miRNA-dependent control of negative regulators of PTI such as Auxin Response Factors 16 and 17 could contribute to this process (Li *et al*., 2010; Figure 6). It is also equally possible that the recently described role of AGO1 in the transcriptional activation of hormone- and stress-responsive genes, including flg22-regulated genes, would contribute to this process (Liu *et al*., 2018). Furthermore, because PAMP-induced oxidative burst is an immediate immune response, it is possible that the miRNA-directed control of ROS production might additionally be caused by the action

of a pre-loaded AGO1-RISC that would operate at the level of early PTI signaling events, an intriguing possibility that will deserve attention in future studies.

Given that the Arabidopsis miRNA pathway is a major component of PTI (Navarro *et al*., 2008; Li *et al*., 2010; this study), it is likely that many pathogen effectors will be found to target this small RNA pathway to enable disease. Consistent with this idea, we have previously identified type-III secreted proteins from *Pto* DC3000 that suppress all the steps of the Arabidopsis miRNA pathway (Navarro *et al*., 2008). However, until now, it was unknown whether some of these BSRs could directly interfere with components of the RNA silencing machinery to suppress miRNA activity and cause disease. In the present work, we show that the bacterial effector HopT1-1 is a critical virulence determinant that promotes growth of *Pto* DC3000 in a physiological context of infection (Figure 1). Importantly, the reduced growth of the *hopT1-1*-deleted strain was fully rescued in miRNA-defective mutants including the *ago1-25, ago1-26* and *ago1-27* mutant alleles (Figures 1 and S1), providing evidence that the Arabidopsis AGO1-dependent miRNA pathway is a major genetic target of HopT1-1. In agreement with these functional analyses, we found that HopT1-1 can physically interact with Arabidopsis AGO1 through two GW motifs, which were found conserved in the putative HopT1-1 ortholog from the phylogenetically distant bacterium *Marinomonas mediterranea* (Figure 2). We also demonstrate that the AGO-binding platform of HopT1-1 plays a central role in the suppression of miRNA activities, as reflected by the derepression of unrelated endogenous miRNA targets, which was specifically observed in HopT1-1 but not in HopT1-1m3 primary transformants (Figure 3). On the contrary, the AGO-binding platform of HopT1-1 moderately interferes with the accumulation of a subset of conserved miRNAs when

expressed in primary transformants (Figure 4). We also found that the constitutive expression of HopT1-1 does not, or negligibly, alter the accumulation of pri-miRNAs (Figure 4). Collectively, our data suggest that the RNA silencing suppression activity of HopT1-1 predominantly acts at the level of AGO1-miRISC activity rather than at the levels of miRNA biogenesis or stability (Figure 6).

In addition, we show that the GW motifs of HopT1-1 are not only essential for the suppression of miRNA activity but also for the dampening of PAMP-triggered H_2O_2 production and of callose deposition in Arabidopsis (Figures 3, 5 and 6). This implies that the BSR activity of HopT1-1 is directly coupled with its ability to suppress PTI. This phenomenon might be due to HopT1-1-induced derepression of negative regulators of PTI that are controlled by miRNAs (Figure 6), and/or to the possible suppression of AGO1-directed transcriptional reprogramming and early PTI signaling mentioned above. Future investigations will be required to determine the detailed mode of action of HopT1-1 once recruited onto AGO1-miRISC. For instance, it will be important to determine whether HopT1-1 could (i) possess an enzymatic activity outside of its AGO-binding platform to impede AGO1 activity, (ii) prevent and/or displace the interaction between AGO1 and yet-unknown endogenous Arabidopsis GW/WG miRNA factors that are relevant for PTI function.

The present study reveals that the use of GW/WG-dependent AGO-binding platforms is not restricted to VSRs (El-Shami *et al.*, 2007; Azevedo *et al*., 2010; Garcia *et al*., 2012; Karran and Sansfaçon, 2014; Aqil *et al*., 2013; Giner *et al*., 2010), but can also be exploited by a functionally relevant bacterial effector. Intriguingly, we have also retrieved GW/WG motifs in an appropriate sequence context in secreted effectors from various phytopathogenic bacteria, fungi and oomycetes (Figure S6). For

instance, we have identified the presence of canonical GW/WG motifs in effectors from the devastating plant bacterial vascular pathogens *Xylella fastidiosa*, *Xanthomonas campestris* pv. *campestris* and *Xanthomonas oryzae pv. oryzae,* or from the oomycetes *Phytophthora sojae* and the Irish potato famine pathogen *Phytophthora infestans* (Figure S6). Canonical GW/WG motifs were also retrieved in effectors produced by the wheat stem rust pathogen *Puccinia graminis* f. sp. *tritici*, which represents one of the most destructive fungal pathogen of wheat worldwide and that was recently shown to encode functional fungal suppressors of RNA silencing (FSR) (Yin *et al.,* 2019), but also by *Fusarium graminearum*, which is the causal agent of Fusarium head blight that causes serious yield losses in wheat and barley worldwide (Figure S6). Collectively, these observations suggest that a wide range of non-viral phytopathogens might have evolved an analogous mode of action to promote pathogenicity in agriculturally relevant crops. It will thus be interesting to establish if the discoveries made on HopT1-1 hold for other silencing suppressors from non-viral phytopathogens. It will also be worth developing innovative strategies to counteract this potentially widespread pathogen-mediated virulence mechanism in order to confer broad spectrum disease resistance in crops.

MATERIALS AND METHODS

DNA Constructs

The pK7WG2D destination vector carrying the *HopT1-1* gene has been previously described (Navarro *et al.*, 2008). To generate the mutated versions of *HopT1-1*, GW>GF substitutions in the *HopT1-1* ORF were carried out by PCR-based site-directed mutagenesis using mismatched primers. The resulting PCR product was

introduced in the pENTR/D-TOPO entry vector (Invitrogen, Carlsbad, CA), sequenced and then recombined into the GATEWAY binary destination vector pK7WG2D using LR clonase (Invitrogen, Carlsbad, CA), to overexpress an untagged protein, or into the GATEWAY binary destination vector pEarleyGate203 to overexpress an Myc fusion protein. Both of the plasmid allow HopT1-1 expression under the control of the constitutive CaMV 35S promoter ($35S_{pro}$). To overexpress HopT1-1 and HopT1-1m3 in the EtHAn system (Thomas *et al.*, 2009), versions of *HopT1-1* and *HopT1-1m3* without a stop codon were cloned in the pENTR/D-TOPO entry vector, which was further recombined with the destination vector pBS0046 containing the *NPTII* promoter. For the BiFC assays, the coding regions of *AGO1*, *SDE3*, *HopT1-1*, *HopT1-1m3* and *HopC1* were first cloned into the pDON207 plasmid and further recombined into the GATEWAY BiFC binary destination vectors pUBN-YFP, containing the N-ter or the C-ter part of YFP protein, that were previously described in Grefen *et al.* (2010). For the FRET-FLIM experiment, the no stop versions of pDON-HopT1-1 and pDON-HopT1-1m3 were recombined into the destination vector pBin-35S-GWY-YFP. For Agrobacterium-mediated transformation in *N. benthamiana*, pDON-HopT1-1 and pDON-HopT1-1m3 were recombined with the GATEWAY pEarleyGate 203 plasmid expressing a MYC tag in N-ter. All the constructs inserted in GATEWAY binary destination vectors were transformed into the *Agrobacterium tumefaciens* strains GV3101 or C58C1.

Transgenic plants and mutants

Arabidopsis thaliana silencing defective mutants *ago1-25, ago1-26, ago1-27*, *ago2-1*, *ago4-2*, *ago4-3*, *dcl2-1 dcl4-2*, *se-1*, *dcl1-11*, *sgs3-1*, *rdr1-1 rdr2-1 rdr6-15* were previously described (Morel *et al.*, 2002; Agorio and Vera, 2007; Havecker *et al.*,

2010; Henderson *et al.*, 2006; Zhang *et al.*, 2008; Mourrain *et al.*, 2000; Garcia-Ruiz, 2010; de Felippes *et al.*, 2011). To generate plants constitutively expressing HopT1-1 and HopT1-1m3 under the control of the 35S promoter, pK7WG2D vectors carrying *HopT1-1* or *HopT1-1m3* sequences were transformed in Col-0 (WT plants) using Agrobacterium-mediated transformation and multiple individual T1 primary transformants (12 or 13 individuals) were analyzed in parallel of WT individual plants.

Bacterial strains

The bacterial strains used in this study include *Pto* DC3000, *HopT1-1*-deleted strain (*Pto* Δ*HopT1-1*) and *HopC1*-deleted strain (*Pto ΔHopC1*). These bacterial strains were grown at 28°C in NYGB medium (5 g L^{-1} bactopeptone, 3 g L^{-1} yeast extract, 20 ml L^{-1} glycerol) containing rifampicin (25 µg/mL) for selection. The *Pto ΔHopT1-1* was generated by an unmarked mutagenesis strategy described by House *et al.* (2004) with some modifications. Briefly, DNA regions upstream and downstream of *HopT1-1* were amplified with primer pairs P4835/P4836 and P4837/P4838 (Table S1), respectively. The resulting PCR fragments were cloned into pENTR/D-TOPO and then recombined into suicide destination vector pMK2016 for the upstream construct, or pMK2017 for the downstream construct, using LR Clonase according to the manufacturer's instructions, resulting in constructs pLN5426 and pLN5472, respectively. Constructs pLN5426 and pLN5472 were integrated into the *Pto* DC3000 chromosome by biparental or triparental mating. Plasmid pBH474, which contains a gene encoding the yeast FLP recombinase, was introduced into the resulting strains to excise the integrated plasmid at FLP recombinase target (FRT) sequences. To cure pBH474, isolated colonies were spread on King's B medium (King *et al.,* 1954) agar plates containing rifampicin (100 µg/mL) with 5% sucrose. PCR primer pair

P4839/P4840 (Table S1) was used to identify mutants that carried the *HopT1-1* deletion. The *Pto ΔHopC1* was generated by an insertional mutagenesis strategy described by Windgassen *et al.* (2000) with some modifications. Briefly, an internal fragment within the *HopC1* coding region was amplified with primer pair P164/P165 (Table S1). The resulting PCR fragment was cloned into a suicide vector pKnockout-Ω that had been digested with XcmI, resulting in construct pLN6. Construct pLN6 was integrated into the *Pto* DC3000 chromosome by triparental mating using spectinomycin (50 µg/mL) to select for the plasmid marker. PCR primer pair P181/P165 was used to identify mutants that contained an integrated pKnockout-Ω in *HopC1*.

Plant Growth Conditions and Treatments

Plants used in this study were grown in growth cabinets at 19–23 °C (dark/light) with an 8-h photoperiod for all the assays. Transgenic plants expressing HopT1-1, under the control of the constitutive CaMV 35S, were selected on plates containing Murashige and Skoog medium (Duchefa) [composition for a 1-L medium (pH = 5.7): 2.3 g MS, 0.5% sucrose, 0.8% agar, 0.5 g MES, vitamins (Sigma)] in presence of Kanamycin (50 µg/mL) and then transferred to soil 15 day-post-germination (dpg). *Nicotiana benthamiana* plants for transient expression assays were grown in growth chamber at 19-23°C (dark/light) with a 16-h photoperiod.

Bacterial growth assays

Five-week-old Col-0 Arabidopsis (WT) or the mutant plants were covered with a lid for 24 hours under high humidity before being dip-inoculated with *Pto* DC3000 WT, *Pto ΔHopT1-1* or *Pto ΔHopC1* at 10^8 cfu/mL with 0,02% of Silwet L-77 (Lehle

Seeds). Dip-inoculated plants were allowed to stay under high humidity condition for 3 days before the bacterial counting was performed. For each condition, around 15 leaves from three plants were collected and the following steps were performed as described in Navarro *et al.* (2008).

Agrobacterium-mediated transient expression

Agrobacterium tumefaciens strains carrying the indicated plasmids were inoculated in 10 ml of LB medium supplied with rifampicin and the other selective antibiotic, and placed in an incubator shaker (200 rpm) at 28°C overnight. Cells were harvested by centrifugation at 4500 rpm and resuspended to a final optical density at 600 nm (OD_{600}) of 0.2 in a solution containing 10 mM MES, pH 5.6, 10 mM $MgCl_2$ and 200 µM acetosyringone. Cultures were incubated in the dark at room temperature for 5 hours before agro-infiltration. For the co-infiltration of two different *A. tumefaciens* strains, equal concentrations (OD_{600}: 0.25) of both cultures were mixed before agro-infiltration of leaves of four-week-old *Nicotiana benthamiana* plants. Infiltrated plants were covered with a lid and the leaves were collected and flash frozen 48-72 hours post-infiltration. Confocal image analyses for the BiFC experiments were performed 2-3 days post infiltration. YFP fluorescence for each sample was visualized and acquired by using Leica SP8 confocal microscopes with a 63x oil immersion objective, and quantification of the fluorescence signal for each picture taken (n=10) was performed using ImageJ software (National Institutes of Health, Bethesda).

Quantitative Real Time PCR analysis

Total RNA was extracted using a phenol-based extraction protocol (Box *et al.*, 2011) followed by DNAse (Promega) digestion at 37°C to remove the genomic DNA. 0.5 µg

of DNAse-digested RNA was reverse-transcribed into cDNA using qScript cDNA Supermix (Quanta Biosciences). The cDNA was quantified using a SYBR Green qPCR mix (Takyon; Eurogentec) and gene-specific primers. PCR was performed in 384-well plates heated at 95 °C for 10 min, followed by 45 cycles of denaturation at 95 °C for 10 s and annealing at 60 °C for 40 s. A melting curve was performed at the end of the amplification. Transcript levels were normalized to that of *Actin2* and/or *Ubiquitin5* levels. Primers used to monitor *Actin2*, *SPL10*, *ARF17, PHB, DCL1, ARF8, ARF10, MYB65, pri-miR159b, pri-miR166a, pri-miR167a, Ub5* and *ALD1* were previously described (Navarro *et al.*, 2008; Zhang *et al.*, 2008; Vaucheret *et al.,* 2004; Vazquez *et al*., 2004; Cai *et al.,* 2018; La Camera *et al.*, 2009). Primer pairs used for the remaining genes are listed in Table S1.

RNA gel blot analyses

Total RNA was extracted from Arabidopsis tissues (5 week-old plants) with Tri-Reagent (Sigma, St. Louis, MO) according to the manufacturer's instructions. RNA gel blot analysis of low molecular weight RNAs was performed on 15-20 µg of total RNAs and as described previously (Navarro *et al.*, 2008). Detection of U6 RNA was used to confirm equal loading. DNA oligonucleotides complementary to miRNA sequences were end-labeled with γ-^{32}P-ATP using T4 PNK (New England Biolabs, Beverly, MA).

Protein extraction and analyses

Total protein extracts were done according to Azevedo *et al.* (2010) resolved on SDS-PAGE after quantification with Bradford Assay. After electroblotting proteins on nitrocellulose membrane (Millipore), protein blot analysis was performed using

antiserum with specific antibodies. Antibodies against AGO1 (AS09527) and PEPC (AS09458) were purchased from Agrisera.

Pull-down experiments

Biotinylated peptides (synthetized by Eurogentec, sequences shown in Figure 2) were mostly insoluble in water and were thus resuspended in 6 M urea, and sonicated four times (Bioruptor^{TM}, Diagenode, 30s on/1min off on High). They were quantified at 205 nm using the Nanodrop 2000 according to the manufacturer's instruction (Thermoscientific) and checked by dot blot analysis. The solubilized peptides were spotted on a nitrocellulose membrane at three different amounts (1 µg, 0.1 µg and 0.01 µg) and were detected by using the streptavidin protein conjugated to HRP (21126, Thermoscientific), and the ECL substrate. For binding assays, 10 µg of peptides were diluted into 450 µL of PBS containing 0.1% of NP-40 and were incubated for 30 min at room temperature in the presence of 0.9 mg of Dynabeads® MyOne™ Streptavidin T1. The beads were then washed once in 0.1% NP-40 PBS and twice in IP buffer (10% glycerol, 50 mM Tris-HCl pH 7.4, 150 mM NaCl, 5 mM $MgCl_2$, 0.1% NP-40, 2 mM DTT, EDTA-free complete Protease Inhibitor Cocktail (Roche)). They were incubated in the presence of inflorescence extracts from Flag-AGO1 Arabidopsis plants in IP buffer for 2 hours at 4°C. After 3 washes of the beads in IP buffer, the proteins were eluted in Laemmli buffer and resolved on a 6% SDS-PAGE gel. The AGO1 protein was detected by Western blot using a Flag-HRP antibody (A8592, Sigma).

FRET-FLIM Measurement

Fluorescence lifetime measurements were performed in time domain using a streak camera (Camborde *et al.,* 2017). The light source is a 440 nm pulsed laser diode (PLP-10, Hamamatsu, Japan) delivering ultrafast picosecond pulses of light at a fundamental frequency of 2 MHz. All images were acquired with a 60x oil immersion lens (plan APO 1.4 N.A., IR) mounted on an inverted microscope (Eclipse TE2000E, Nikon, Japan). The fluorescence emission is directed back into the detection unit through a short pass filter and a band pass filter (490/30 nm). The detector is a streak camera (Streakscope C4334, Hamamatsu Photonics, Japan) coupled to a fast and high-sensitivity CCD camera (model C8800-53C, Hamamatsu). For each acquisition, average fluorescence decay profiles were plotted and lifetimes were estimated by fitting data with exponential function using a non-linear least-squares estimation procedure (Camborde *et al.*, 2017). Fluorescence lifetime of the donor was experimentally measured in the presence and absence of the acceptor. FRET efficiency (E) was calculated by comparing the lifetime of the donor in the presence (τ_{DA}) or absence (τ_D) of the acceptor: $E=1-(\tau_{DA})/(\tau_D)$. Statistical comparisons between control (donor) and assay (donor + acceptor) lifetime values were performed by Student *t* test.

Quantification of flg22-induced ROS production

For each condition, discs (0.4 cm in diameter) of leaf tissue were harvested from three individual five-week-old plants and incubated in water in 96-well plates overnight in a growth chamber at 23°C. After 24 hours, the water was removed and replaced by 100 µL of H_2O containing 20 µM luminol and 1 µg of horseradish peroxidase (Sigma) with 100 nM flg22. Luminescence (relative light units) was

immediately measured for a time-course of 45 min using a Tristar LB 941 plate reader (Berthold technologies).

Callose deposition

Five-week-old Arabidopsis Col-0 (WT) plants or *ago1-27* mutant plants were infiltrated with 10 mM of $MgCl_2$ or 10^8 cfu/mL (OD_{600}: 0.2) of EtHAn strains. Seven hours after infiltration, around 12 leaves were collected from three independent plants and incubated overnight in lactophenol (1 volume of glycerol:lactic acid:phenol:water, ratio 1:1:1:1, and 2 volumes of EtOH). After a first washing step in 50% EtOH and a second one in water, leaves were incubated for 30 min in aniline blue staining solution (150 mM K_2HPO_4 pH 9.5 with 0.01% aniline blue). Leaves were mounted with 50% glycerol and visualized with Olympus Macro Zoom System Microscope MVX10 fluorescent microscope (excitation filter 365 nm and barrier filter 420 nm). The number of callose deposits was quantified using ImageJ software. Forty fields of view (each 0.56 mm^2) were analyzed and averaged.

DAB staining assay

Five-week-old Arabidopsis Col-0 (WT) plants or *ago1-27* mutant plants were infiltrated with 10 mM of $MgCl_2$ or 10^8 cfu/mL (OD_{600}: 0.2) of EtHAn strains. After 48 hours, the infiltrated leaves were collected and vacuum-infiltrated with DAB staining buffer (1 mg/mL, pH 3.5) and then incubated for 5 hours in the same buffer. Leaves were boiled for 15 min in an EtOH:glycerol:acid lactic (ratio 4:1:1) solution, washed overnight in EtOH and then mounted with 50% glycerol and further visualized using Olympus Macro Zoom System Microscope MVX10. The intensity of DAB staining

was quantified with ImageJ software. Forty fields of view (each 0.56 mm^2) were analyzed and averaged.

REFERENCES

Agorio, A., and Vera, P. (2007). ARGONAUTE4 is required for resistance to *Pseudomonas syringae* in Arabidopsis. The Plant Cell *19*, 3778-3790.

Allen, E., Xie, Z., Gustafson, A.M., and Carrington, J.C. (2005). microRNA-directed phasing during trans-acting siRNA biogenesis in plants. Cell 121, 207-221.

Aqil, M., Naqvi, A.R., Bano, A.S., and Jameel, S. (2013). The HIV-1 Nef protein binds argonaute-2 and functions as a viral suppressor of RNA interference. PLoS one *8*, e74472.

Arribas-Hernandez, L., Marchais, A., Poulsen, C., Haase, B., Hauptmann, J., Benes, V., Meister, G., and Brodersen, P. (2016). The Slicer Activity of ARGONAUTE1 Is Required Specifically for the Phasing, Not Production, of Trans-Acting Short Interfering RNAs in Arabidopsis. The Plant cell 28, 1563-1580.

Azevedo, J., Garcia, D., Pontier, D., Ohnesorge, S., Yu, A., Garcia, S., Braun, L., Bergdoll, M., Hakimi, M.A., Lagrange, T., et al. (2010). Argonaute quenching and global changes in Dicer homeostasis caused by a pathogen-encoded GW repeat protein. Genes & Dev. 24, 904-915.

Azevedo, J., Cooke, R., and Lagrange, T. (2011). Taking RISCs with Ago hookers. Curr Opin Plant Biol. *14*, 594-600.

Baulcombe, D.C. (2015). VIGS, HIGS and FIGS: small RNA silencing in the interactions of viruses or filamentous organisms with their plant hosts. Current opinion in plant biology *26*, 141-146.

Block, A. and Alfano, JR. (2011). Plant targets for *Pseudomonas syringae* type III effectors: virulence targets or guarded decoys? Cell Opin Microbiol *14*, 39-46.

Bohmert, K., Camus, I., Bellini, C., Bouchez, D., Caboche, M., and Benning, C. (1998). AGO1 defines a novel locus of Arabidopsis controlling leaf development. The EMBO journal 17, 170-180.

Bologna, N.G., and Voinnet, O. (2014). The diversity, biogenesis, and activities of endogenous silencing small RNAs in Arabidopsis. Annual review of plant biology *65*, 473-503.

Box, M.S., Coustham, V., Dean, C., and Mylne, J.S. (2011). Protocol: A simple phenol-based method for 96-well extraction of high-quality RNA from Arabidopsis. Plant methods *7*, 7.

Brodersen, P., Sakvarelidze-Achard, L., Bruun-Rasmussen, M., Dunoyer, P., Yamamoto, Y.Y., Sieburth, L., and Voinnet, O. (2008). Widespread translational inhibition by plant miRNAs and siRNAs. Science *320*, 1185-1190.

Brosseau, C., El Oirdi, M., Adurogbangba, A., Ma, X., and Moffett, P. (2016). Antiviral Defense Involves AGO4 in an Arabidopsis-Potexvirus Interaction. Molecular plant-microbe interactions: MPMI *29*, 878-888.

Cai, Q., Liang, C., Wang, S., Hou, Y., Gao, L., Liu, L., ... & Chen, X. (2018). The disease resistance protein SNC1 represses the biogenesis of microRNAs and phased siRNAs. Nature communications, *9* (1), 1-14.

Camborde L., Jauneau A., Brière C., Deslandes L., Dumas B., Gaulin E. (2017). Detection of nucleic acid-protein interactions in plant leaves using fluorescence lifetime imaging microscopy. Nat Protoc. 12(9):1933-1950.

Carbonell, A., Fahlgren, N., Garcia-Ruiz, H., Gilbert, K.B., Montgomery, T.A., Nguyen, T., Cuperus, J.T., and Carrington, J.C. (2012). Functional analysis of three

Arabidopsis ARGONAUTES using slicer-defective mutants. The Plant cell *24*, 3613-3629.

Chen, X. (2004). A microRNA as a translational repressor of APETALA2 in Arabidopsis flower development. Science *303*, 2022-2025.

Couto, D., Zipfel, C. (2016). Regulation of pattern recognition receptor signaling in plants. Nat Rev Immunol. 16, 537-552.

Dalmay, T., Hamilton, A., Rudd, S., Angell, S., and Baulcombe, D.C. (2000). An RNA-dependent RNA polymerase gene in Arabidopsis is required for posttranscriptional gene silencing mediated by a transgene but not by a virus. Cell *101*, 543-553.

de Felippes, F.F., Ott, F., and Weigel, D. (2011). Comparative analysis of non-autonomous effects of tasiRNAs and miRNAs in Arabidopsis thaliana. Nucleic acids research *39*, 2880-2889.

Deleris, A., Gallego-Bartolome, J., Bao, J., Kasschau, K.D., Carrington, J.C., and Voinnet, O. (2006). Hierarchical action and inhibition of plant Dicer-like proteins in antiviral defense. Science *313*, 68-71.

Derrien, B., Baumberger, N., Schepetilnikov, M., Viotti, C., De Cillia, J., Ziegler-Graff, V., Isono, E., Schumacher, K., and Genschik, P. (2012). Degradation of the antiviral component ARGONAUTE1 by the autophagy pathway. Proceedings of the National Academy of Sciences of the United States of America *109*, 15942-15946.

Diaz-Pendon, J.A., Li, F., Li, W.X., and Ding, S.W. (2007). Suppression of antiviral silencing by cucumber mosaic virus 2b protein in Arabidopsis is associated with drastically reduced accumulation of three classes of viral small interfering RNAs. The Plant cell *19*, 2053-2063.

Donaire, L., Barajas, D., Martinez-Garcia, B., Martinez-Priego, L., Pagan, I., and Llave, C. (2008). Structural and genetic requirements for the biogenesis of tobacco rattle virus-derived small interfering RNAs. Journal of virology *82*, 5167-5177.

El-Shami, M., Pontier, D., Lahmy, S., Braun, L., Picart, C., Vega, D., Hakimi, M.A., Jacobsen, S.E., Cooke, R., and Lagrange, T. (2007). Reiterated WG/GW motifs form functionally and evolutionarily conserved ARGONAUTE-binding platforms in RNAi-related components. Genes & development *21*, 2539-2544.

Fagard, M., Boutet, S., Morel, J.B., Bellini, C., and Vaucheret, H. (2000). AGO1, QDE-2, and RDE-1 are related proteins required for post-transcriptional gene silencing in plants, quelling in fungi, and RNA interference in animals. Proceedings of the National Academy of Sciences of the United States of America 97, 11650-11654.

Fahlgren, N., Howell, M.D., Kasschau, K.D., Chapman, E.J., Sullivan, C.M., Cumbie, J.S., Givan, S.A., Law, T.F., Grant, S.R., Dangl, J.L.*, et al.* (2007). High-throughput sequencing of Arabidopsis microRNAs: evidence for frequent birth and death of MIRNA genes. PloS one *2*, e219.

Fei, Q., Xia, R., and Meyers, B.C. (2013). Phased, secondary, small interfering RNAs in posttranscriptional regulatory networks. The Plant cell 25, 2400-2415.

Felix, G., Duran, J.D., Volko, S., and Boller, T. (1999). Plants have a sensitive perception system for the most conserved domain of bacterial flagellin. Plant journal, 265-276.

Finnegan, E.J., Margis, R., and Waterhouse, P.M. (2003). Posttranscriptional gene silencing is not compromised in the Arabidopsis CARPEL FACTORY (DICER-LIKE1) mutant, a homolog of Dicer-1 from Drosophila. Current biology : CB *13*, 236-240.

Garcia, D., Garcia, S., Pontier, D., Marchais, A., Renou, J. P., Lagrange, T., & Voinnet, O. (2012). Ago hook and RNA helicase motifs underpin dual roles for SDE3 in antiviral defense and silencing of nonconserved intergenic regions. Molecular cell, 48(1), 109-120.

Garcia-Ruiz, H., A. Takeda, E. J. Chapman, C. M. Sullivan, N. Fahlgren, K. J. Brempelis, and J. C. Carrington. (2010). "Arabidopsis RNA-dependent RNA polymerases and dicer-like proteins in antiviral defense and small interfering RNA biogenesis during Turnip Mosaic Virus infection.Plant Cell 22 (2):481-96.

Giner, A., Lakatos, L., García-Chapa, M., López-Moya, JJ., and Burgyán, J. (2010). Viral protein inhibits RISC activity by argonaute binding through conserved GW/WG motifs. PLoS Pathog. 15, e1000996.

Gómez-Gómez, L., Felix, G., and Boller, T. (1999). A single locus determines sensitivity to bacterial flagellin in *Arabidopsis thaliana*. Plant J. 18, 277-84.

Gómez-Gómez, L., Boller, T. (2000). FLS2: an LRR receptor-like kinase involved in the perception of the bacterial elicitor flagellin in Arabidopsis. Mol Cell. 5, 1003-11.

Grefen, C., N. Donald, K. Hashimoto, J. Kudla, K. Schumacher, and M. R. Blatt. 2010. "A ubiquitin-10 promoter-based vector set for fluorescent protein tagging facilitates temporal stability and native protein distribution in transient and stable expression studies." *Plant J* 64 (2):355-65.

Gryczynski, Z., Gryczynski, I., and Lakowicz, J. R., (2005) Basics of Fluorescence and FRET., in *Molecular Imaging: FRET Microscopy and Spectroscopy*, Periasamy, A. and Day, R. N. (eds.), Oxford University Press, New York, pages 21-56.

Guo, M., Chancey, S.T., Tian, F., Ge, Z., Jamir, Y., and Alfano, J.R. (2005). *Pseudomonas syringae* type III chaperones ShcO1, ShcS1, and ShcS2 facilitate translocation of their cognate effectors and can substitute for each other in the secretion of HopO1-1. Journal of bacteriology *187*, 4257-4269.

Hamilton, A.J., and Baulcombe, DC. (1999). A species of small antisense RNA in posttranscriptional gene silencing in plants. Science *286*, 950-952.

Harvey, J.J., Lewsey, M.G., Patel, K., Westwood, J., Heimstadt, S., Carr, J.P., and Baulcombe, D.C. (2011). An antiviral defense role of AGO2 in plants. PloS one *6*, e14639.

Hauck, P., Thilmony, R., and He SY. (2003). A *Pseudomonas syringae* type III effector suppresses cell wall-based extracellular defense in susceptible Arabidopsis plants. (2003). Proc Natl Acad Sci U S A. *100*, 8577-82.

Havecker, E. R., L. M. Wallbridge, T. J. Hardcastle, M. S. Bush, K. A. Kelly, R. M. Dunn, F. Schwach, J. H. Doonan, and D. C. Baulcombe. 2010. "The Arabidopsis RNA-directed DNA methylation argonautes functionally diverge based on their expression and interaction with target loci." *Plant Cell* 22 (2):321-34.

Henderson, I. R., X. Zhang, C. Lu, L. Johnson, B. C. Meyers, P. J. Green, and S. E. Jacobsen. 2006. "Dissecting Arabidopsis thaliana DICER function in small RNA processing, gene silencing and DNA methylation patterning." *Nat Genet* 38 (6):721-5.

Hong, J.K., Kang, S.R., Kim, Y.H., Yoon, D.J., Kim, D.H., Kim, H.J., Sung, C.H., Kang, H.S., Choi, C.W., Kim, S.H.*, et al*. (2013). Hydrogen Peroxide- and Nitric Oxide-mediated Disease Control of Bacterial Wilt in Tomato Plants. The plant pathology journal *29*, 386-396.

Hou, Y., Zhai, Y., Feng, L., Karimi, H.Z., Rutter, B.D., Zeng, L., Choi, D.S., Zhang, B., Gu, W., Chen, X., et al. (2019). A Phytophthora Effector Suppresses Trans-Kingdom RNAi to Promote Disease Susceptibility. Cell host & microbe 25, 153-165 e155.

House, B. L., M. W. Mortimer, and M. L. Kahn. 2004. "New recombination methods for *Sinorhizobium meliloti* genetics." *Appl Environ Microbiol* 70 (5):2806-15.

Jaubert, M., Bhattacharjee, S., Mello, A.F., Perry, K.L., and Moffett, P. (2011). ARGONAUTE2 mediates RNA-silencing antiviral defenses against Potato virus X in Arabidopsis. Plant physiology *156*, 1556-1564.

Jones, J.D., and Dangl, J.L. (2006). The plant immune system. Nature *444*, 323-329.

Jones, J.D., Vance, R.E., and Dangl, J.L. (2016). Intracellular innate immune surveillance devices in plants and animals. Science *354*.

Karran, R.A., and Sanfaçon, H. (2014). Tomato ringspot virus coat protein binds to ARGONAUTE 1 and suppresses the translation repression of a reporter gene. Molecular plant-microbe interactions: MPMI *27*, 933-943.

Katiyar-Agarwal, S., Morgan, R., Dahlbeck, D., Borsani, O., Villegas, A., Jr., Zhu, J.K., Staskawicz, B.J., and Jin, H. (2006). A pathogen-inducible endogenous siRNA in plant immunity. Proceedings of the National Academy of Sciences of the United States of America *103*, 18002-18007.

Katiyar-Agarwal, S., Gao, S., Vivian-Smith, A., and Jin, H. (2007). A novel class of bacteria-induced small RNAs in Arabidopsis. Genes & development *21*, 3123-3134.

King, E. O., M. K. Ward, and D. E. Raney. 1954. "Two simple media for the demonstration of pyocyanin and fluorescin." *J Lab Clin Med* 44 (2):301-7.

Kurihara, Y., and Watanabe, Y. (2004). Arabidopsis micro-RNA biogenesis through Dicer-like 1 protein functions. Proceedings of the National Academy of Sciences of the United States of America *101*, 12753-12758.

La Camera, S., C. Balague, C. Gobel, P. Geoffroy, M. Legrand, I. Feussner, D. Roby, and T. Heitz. 2009. "The Arabidopsis patatin-like protein 2 (PLP2) plays an essential role in cell death execution and differentially affects biosynthesis of oxylipins and resistance to pathogens." *Mol Plant Microbe Interact* 22 (4):469-81.

Li, X., Lin, H., Zhang, W., Zou, Y., Zhang, J., Tang, X., and Zhou, J.M. (2005). Flagellin induces innate immunity in nonhost interactions that is suppressed by *Pseudomonas syringae* effectors. Proceedings of the National Academy of Sciences of the United States of America *102*, 12990-12995.

Li, Y., Zhang, Q., Zhang, J., Wu, L., Qi, Y., and Zhou, J.M. (2010). Identification of microRNAs involved in pathogen-associated molecular pattern-triggered plant innate immunity. Plant physiology *152*, 2222-2231.

Li, L., Yu, Y., Zhou, Z., and Zhou, J.M. (2016). Plant pattern-recognition receptors controlling innate immunity. Sci China Life Sci. 59, 1350.

Liu, C., Xin, Y., Xu, L., Cai, Z., Xue, Y., Liu, Y., Xie, D., Liu, Y., and Qi, Y. (2018). Arabidopsis ARGONAUTE 1 Binds Chromatin to Promote Gene Transcription in Response to Hormones and Stresses. Developmental cell *44*, 348-361 e347.

Llave, C., Kasschau, K.D., Rector, M.A., and Carrington, J.C. (2002). Endogenous and silencing-associated small RNAs in plants. The Plant cell *14*, 1605-1619.

Lobbes, D., Rallapalli, G., Schmidt, DD., Martin, C., Clarke, J. (2006). SERRATE: a new player on the plant microRNA scene. EMBO Rep. *7*, 1052-1058.

Mallory, A.C., Hinze, A., Tucker, M.R., Bouche, N., Gasciolli, V., Elmayan, T., Lauressergues, D., Jauvion, V., Vaucheret, H., and Laux, T. (2009). Redundant and specific roles of the ARGONAUTE proteins AGO1 and ZLL in development and small RNA-directed gene silencing. PLoS genetics 5, e1000646.

Misas-Villamil, J.C., Kolodziejek, I., and van der Hoorn, R.A. (2011). *Pseudomonas syringae* colonizes distant tissues in *Nicotiana benthamiana* through xylem vessels. The Plant journal: for cell and molecular biology *67*, 774-782.

Morel, J.B., Godon, C., Mourrain, P., Beclin, C., Boutet, S., Feuerbach, F., Proux, F., and Vaucheret, H. (2002). Fertile hypomorphic ARGONAUTE (ago1) mutants

impaired in post-transcriptional gene silencing and virus resistance. The Plant cell *14*, 629-639.

Mourrain, P., Beclin, C., Elmayan, T., Feuerbach, F., Godon, C., Morel, J.B., Jouette, D., Lacombe, A.M., Nikic, S., Picault, N.*, et al.* (2000). Arabidopsis SGS2 and SGS3 genes are required for posttranscriptional gene silencing and natural virus resistance. Cell *101*, 533-542.

Navarro, L., Zipfel, C., Rowland, O., Keller, I., Robatzek, S., Boller, T., and Jones, J.D. (2004). The transcriptional innate immune response to flg22. Interplay and overlap with Avr gene-dependent defense responses and bacterial pathogenesis. Plant physiology *135*, 1113-1128.

Navarro, L., Dunoyer, P., Jay, F., Arnold, B., Dharmasiri, N., Estelle, M., Voinnet, O., and Jones, J.D. (2006). A plant miRNA contributes to antibacterial resistance by repressing auxin signaling. Science *312*, 436-439.

Navarro, L., Jay, F., Nomura, K., He, S.Y., and Voinnet, O. (2008). Suppression of the microRNA pathway by bacterial effector proteins. Science *321*, 964-967.

Nuthikattu, S., McCue, A.D., Panda, K., Fultz, D., DeFraia, C., Thomas, E.N., and Slotkin, R.K. (2013). The initiation of epigenetic silencing of active transposable elements is triggered by RDR6 and 21-22 nucleotide small interfering RNAs. Plant physiology 162, 116-131.

Palatnik, J.F., Allen, E., Wu, X., Schommer, C., Schwab, R., Carrington, J.C., and Weigel, D. (2003). Control of leaf morphogenesis by microRNAs. Nature *425*, 257-263.

Park, W., Li, J., Song, R., Messing, J., and Chen, X. (2002). CARPEL FACTORY, a Dicer homolog, and HEN1, a novel protein, act in microRNA metabolism in Arabidopsis thaliana. Current biology: CB *12*, 1484-1495.

Poulsen, C., Vaucheret, H., Brodersen, P. (2013). Lessons on RNA silencing mechanisms in plants from eukaryotic argonaute structures. Plant Cell 25, 22-37.

Pumplin, N., and Voinnet, O. (2013). RNA silencing suppression by plant pathogens: defence, counter-defence and counter-counter-defence. Nature reviews. Microbiology *11*, 745-760.

Qiao, Y., Liu, L., Xiong, Q., Flores, C., Wong, J., Shi, J., Wang, X., Liu, X., Xiang, Q., Jiang, S*., et al.* (2013). Oomycete pathogens encode RNA silencing suppressors. Nature genetics *45*, 330-333.

Qiao, Y., Shi, J., Zhai, Y., Hou, Y., and Ma, W. (2015). Phytophthora effector targets a novel component of small RNA pathway in plants to promote infection. Proceedings of the National Academy of Sciences of the United States of America *112*, 5850-5855.

Rajagopalan, R., Vaucheret, H., Trejo, J., and Bartel, D.P. (2006). A diverse and evolutionarily fluid set of microRNAs in Arabidopsis thaliana. Genes Dev. *20*: 3407-3425.

Rhoades, M.W., Reinhart, B.J., Lim, L.P., Burge, C.B., Bartel, B., and Bartel, D.P. (2002). Prediction of plant microRNA targets. Cell *110*, 513-520.

Staiger, D., Korneli, C., Lummer, M., and Navarro, L. (2013). Emerging role for RNA-based regulation in plant immunity. New Phytol. *197*, 394-404.

Thomas, W.J., Thireault, C.A., Kimbrel, J.A., and Chang, J.H. (2009) Recombineering and stable integration of the *Pseudomonas syringae* pv. *syringae* 61 hrp/hrc cluster into the genome of the soil bacterium *Pseudomonas fluorescens* Pf0-1. Plant J. *60*, 919-928.

Till, S., Lejeune, E., Thermann, R., Bortfeld, M., Hothorn, M., Enderle, D., Heinrich, C.,Hentz,M.W. and Ladurner, A. G. (2007). A conserved motif in Argonaute-

interacting proteins mediates functional interactions through the Argonaute PIWI domain. Nature structural & molecular biology, *14*(10), 897-903.

Torres, M.A., Jones, J.D., and Dangl, J.L. (2006). Reactive oxygen species signaling in response to pathogens. Plant Physiol. 141, 373-378.

Tsuda, K., and Katagiri, F. (2010). Comparing signaling mechanisms engaged in pattern-triggered and effector-triggered immunity. Current opinion in plant biology *13*, 459-465.

Vaucheret, H., Vazquez, F., Crete, P., and Bartel, D.P. (2004). The action of ARGONAUTE1 in the miRNA pathway and its regulation by the miRNA pathway are crucial for plant development. Genes and development *18*, 1187-1197.

Vaucheret, H. (2008). Plant ARGONAUTES. Trends Plant Sci. *13*, 350-358.

Vazquez, F., Gasciolli, V., Crete, P., and Vaucheret, H. (2004). The nuclear dsRNA binding protein HYL1 is required for microRNA accumulation and plant development, but not posttranscriptional transgene silencing. *Current biology* : CB *14*, 346-351.

Wang, M., Weiberg, A., Lin, F. M., Thomma, B. P., Huang, H. D., & Jin, H. (2016). Bidirectional cross-kingdom RNAi and fungal uptake of external RNAs confer plant protection. *Nature plants*, *2*(10), 1-10.

Weiberg, A., & Jin, H. (2015). Small RNAs, the secret agents in the plant–pathogen interactions. *Current opinion in plant biology*, *26*, 87-94.

Windgassen, M., A. Urban, and K. E. Jaeger. 2000. "Rapid gene inactivation in Pseudomonas aeruginosa." *FEMS Microbiol Lett* 193 (2):201-5.

Wong, J., Gao, L., Yang, Y., Zhai, J., Arikit, S., Yu, Y., Duan, S., Chan, V., Xiong, Q., Yan, J.*, et al.* (2014). Roles of small RNAs in soybean defense against *Phytophthora sojae* infection. The Plant journal: for cell and molecular biology *79*, 928-940.

Xie, Z., Kasschau, K.D., and Carrington, J.C. (2003). Negative feedback regulation of Dicer-Like1 in Arabidopsis by microRNA-guided mRNA degradation. Curr Biol. *13*, 784-789.

Xie, Z., Johansen, L.K., Gustafson, A.M., Kasschau, K.D., Lellis, A.D., Zilberman, D., Jacobsen, S.E., and Carrington, J.C. (2004). Genetic and functional diversification of small RNA pathways in plants. PLoS biology *2*, E104.

Xie, Z., Allen, E., Wilken, A., and Carrington, J.C. (2005). DICER-LIKE 4 functions in trans-acting small interfering RNA biogenesis and vegetative phase change in *Arabidopsis thaliana*. Proceedings of the National Academy of Sciences of the United States of America 102, 12984-12989.

Yang, L., Liu, Z., Lu, F., Dong, A., and Huang, H. (2006). SERRATE is a novel nuclear regulator in primary microRNA processing in Arabidopsis. The Plant journal : for cell and molecular biology 47, 841-850.

Yin, C., Ramachandran, S.R., Zhai, Y., Bu, C., Pappu, H.R., and Hulbert, S.H. (2019). A novel fungal effector from *Puccinia graminis* suppressing RNA silencing and plant defense responses. The New phytologist *222*, 1561-1572.

Yu, A., Lepere, G., Jay, F., Wang, J., Bapaume, L., Wang, Y., Abraham, A.L., Penterman, J., Fischer, R.L., Voinnet, O.*, et al.* (2013). Dynamics and biological relevance of DNA demethylation in Arabidopsis antibacterial defense. Proceedings of the National Academy of Sciences of the United States of America *110*, 2389-2394.

Zhang, X., Yuan, Y.R., Pei, Y., Lin, S.S., Tuschl, T., Patel, D.J., and Chua, N.H. (2006). Cucumber mosaic virus-encoded 2b suppressor inhibits Arabidopsis Argonaute1 cleavage activity to counter plant defense. Genes & development *20*, 3255-3268.

Zhang, JF., Yuan, LJ., Shao, Y., Du, W., Yan, DW., and Lu, YT. (2008). The disturbance of small RNA pathways enhanced abscisic acid response and multiple stress responses in Arabidopsis. Plant Cell Environ. 31, 562-74.

Zhang, X., Zhao, H., Gao, S., Wang, W.C., Katiyar-Agarwal, S., Huang, H.D., Raikhel, N., and Jin, H. (2011). Arabidopsis Argonaute 2 regulates innate immunity via miRNA393(∗)-mediated silencing of a Golgi-localized SNARE gene, MEMB12. Mol Cell. *42*, 356-366.

Zielezinski, A., and Karlowski, W.M. (2015). Integrative data analysis indicates an intrinsic disordered domain character of Argonaute-binding motifs. Bioinformatics *31*, 332-339.

Zipfel, C., Robatzek, S., Navarro, L., Oakeley, E.J., Jones, J.D., Felix, G., and Boller, T. (2004). Bacterial disease resistance in Arabidopsis through flagellin perception. Nature *428*, 764-767.

Zipfel, C., Kunze, G., Chinchilla, D., Caniard, A., Jones, JD., Boller, T., Felix, G. (2006). Perception of the bacterial PAMP EF-Tu by the receptor EFR restricts *Agrobacterium*-mediated transformation. *Cell* 125, 749-60.

FIGURE LEGENDS

Figure 1. The growth defect of the *hopT1-1*-deleted strain of *Pto* DC3000 is specifically rescued in Arabidopsis miRNA-defective mutants

Five-week-old Col-0 Arabidopsis (WT) plants and indicated genotypes were dip-inoculated with bacterial strains *Pto* DC3000 (*Pto*) (blue dots) and *Pto ΔhopT1-1* (green dots) or *Pto ΔhopC1* (orange dots) at a concentration of 10^8 cfu/mL. At three days post-inoculation (3 dpi), leaves from three plants were collected and bacterial titers were further monitored. Each dot represents a number of bacteria as log (cfu per cm^2) and mean (n=8 or 16) is represented as horizontal line. Similar results were obtained in two to three independent experiments (results from biological replicates are provided in Figure S1). **(A)** Left panel: growth of wild type *Pto* DC3000 strain

(*Pto*) and of *hopT1-1* deleted bacterial strain (***Pto ΔhopT1-1)*** in WT plants and in three different hypomorphic *ago1* mutants, namely *ago1-25*, *ago1-26* and *ago1-27*. Right panel: growth of wild type *Pto* DC3000 strain (*Pto*) and of *hopC1*-deleted bacterial strain (***Pto ΔhopC1)*** in WT plants and in *ago1-27* mutant. **(B)** Growth of WT *Pto* and of ***Pto ΔhopT1-1*** in WT plants and in mutants defective in AGO2 (*ago2-1*) or in AGO4 (*ago4-2* and *ago4-3*). **(C)** Same as in (A-Left panel) but in miRNA biogenesis-defective mutants *se-1* and *dcl1-11*. **(D)** Same as in (B) but in siRNA biogenesis mutants: *sgs3-1, rdr1-1 rdr2-1 rdr6-15* and *dcl2-1 dcl4-2.* Statistical significance was assessed using the ANOVA test (n.s.: p-value > 0.05; *: p-value < 0.05; **: p-value < 0.01; ***: p-value < 0.001; ****: p-value < 0.0001).

Figure 2. HopT1-1 possesses two conserved GW motifs that are required for HopT1-1-AGO1 interaction

(A) Partial sequences (69-210 amino acids) of the *Pto* DC3000 HopT1-1 (NP_808678.1) and the *Marinomonas mediterranea* MMB-1 HopT1-1 (WP_013659626.1) proteins were aligned using clustalW2. These protein sequences possess three conserved GW motifs (named GW1, GW2 and GW3) highlighted in black boxes. The score of GW motifs prediction was retrieved by using the matrix AGO-planVir of the web portal http://150.254.123.165/whub/ (Zielezinski A. & Karlowski WM, 2015) and is indicated below each GW motif. **(B)** BiFC assay in *N. benthamiana*. Four-week-old *N. benthamiana* were co-infiltrated with combinations of *Agrobacterium tumefaciens* strains carrying different constructs fused with N-terminal or C-terminal part of YFP. Interaction of NYFP-AGO1 with CYFP-HopT1-1 (left bottom) or with CYFP-HopT1-1m3 (right bottom) was tested. As negative controls, NYFP-AGO1 was co-infiltrated with CYFP-HopC1 (left top) and NYFP-SDE3 was co-

infiltrated with cYFP-HopT1-1 (right top). YFP fluorescence was visualized by confocal microscopy three days post-infiltration (left panel) and quantification of the fluorescence signal for each picture taken (n=10) was performed using ImageJ software (right panel). Each dot represents the intensity of fluorescence signal in epidermal cells (white arrow) resulting from the interaction of each pair of combination as indicated in the dot plot. The signal in stomata cells is likely due to autofluorescence and should thus not be considered as positive BiFC signal. Two biological replicates are presented and the mean is represented as the horizontal line. Statistical significance was assessed using the ANOVA test (n.s.: p-value>0.05; ****: p-value<0.0001). **(C)** FRET-FLIM measurements showing that HopT1-1, but not HopT1-1m3, interacts with AGO1 in the cytoplasm of plant cells. Mean lifetime, τ, is in nanoseconds (ns). [(a)] For each cell analyzed, average fluorescence decay profiles measured in the cytoplasm were plotted and fitted with exponential function using a non-linear square estimation procedure, and the mean lifetime was calculated according to $\tau=\sum_i \tau_i^2/\sum_i \tau_i$ with $I(t) = \sum \alpha_i e^{-t/\tau i}$, standard error of the mean, [(b)] $\Delta t=\tau_D-\tau_{DA}$ (in ps), [(c)] total number of measured cell cytoplasm, and [(d)] % FRET efficiency: $E = 1 – (\tau_{DA}/\tau_D)$. p-value of the difference between the donor lifetimes in the presence and in the absence of acceptor (Student's *t* test) is indicated. **(D)** To assess which GW motif/s of HopT1-1 is/are required for the interaction with AGO1, synthetic biotinylated peptides containing the WT (GW) or the mutated version (GF) of each GW motif of HopT1-1 were mobilized on streptavidin magnetic beads. Specific peptide-loaded beads were further incubated with total protein extracted from Flag-AGO1 inflorescence. The presence of Flag-AGO1 in the total protein extract (input) and bound to the beads was assessed by immunoblotting. The peptides GW2 and GW3, but not GW1, can interact with Flag-AGO1. This interaction was partially or

completely impaired in presence of GF2 and GF3, respectively.

Figure 3. HopT1-1 suppresses AGO1-mediated miRNA function in a GW-dependent manner

(A) HopT1 expression level was monitored by RT-qPCR analysis in individual five-week-old primary transformants expressing HopT1-1 or HopT1-1m3 under the constitutive 35S promoter. Number of individuals analyzed in each condition is n=13. *Actin* was used as a control. **(B)** Expression of endogenous miRNA targets was monitored by RT-qPCR analysis in the same HopT1-1 transgenic plants as well as in individual WT and *ago1-27* mutant plants. The miRNA that targets the analyzed transcript is indicated between brackets. *Actin* was used as a control. **(C)** Relative mRNA accumulation levels of RNA silencing factors targeted by miRNAs were monitored by RT-qPCR analysis in the same plants described in (B). AGO4 was used as an internal control, as this silencing factor is not targeted by any miRNA. *Actin* was used as a control. Statistical significance was assessed by comparing the mean (black bar) of each condition with the mean of WT condition, using one-way ANOVA analysis (*: p-value < 0.05; **: p-value < 0.01; ***: p-value < 0.001; ****: p-value < 0.0001). **(D)** Individuals of the plants depicted in (B) were pooled to monitor by immunoblotting the protein accumulation levels of the RNA silencing factors depicted in (C). PEPC protein accumulation level was used as loading control for each blot. Presence of DCL1 and AGO4 proteins was revealed using the same blot. Relative quantification of the protein accumulation using PEPC accumulation level was done using ImageJ software and is indicated below each condition. Another biological replicate is shown from other individuals of plants in Figure S4.

Figure 4. The AGO-binding platform of HopT1-1 triggers a moderate decrease in the accumulation of a subset of conserved miRNAs, while it does not, or negligibly, interfere with the processing of cognate pri-miRNAs

(A) Top panel: accumulation levels of endogenous miRNAs in pooled WT plants and in pooled primary transformants expressing HopT1-1 or HopT1-1m3 were assessed by northern blot. U6 was used as a loading control. Relative quantification of each miRNA accumulation using U6 accumulation level was done using ImageJ software and is indicated below each condition. Bottom panel: quantification of the miRNA accumulation level in HopT1-1 and in HopT1-1m3 plants relative to the miRNA accumulation in WT plants is shown for two biological replicates (Figures 4A and S5A). **(B)** Accumulation levels of endogenous pri-miRNAs were assessed by RT-qPCR in five-week-old WT plants and in *dcl1-11* and *se-1* mutants (top panels) or in the plants described in Figure 3A (bottom panels). *Ubiquitin5 (ub5)* was used as a control. For the RT-qPCR analysis of HopT1-1 and HopT1-1m3 transgenic plants, statistical significance was assessed by comparing the mean (black bar) of each condition with the mean of WT condition, using one-way ANOVA analysis (*: p-value < 0.05; **: p-value < 0.01; ***: p-value < 0.001).

Figure 5. HopT1-1 dampens PTI in a GW-dependent manner and its presence mimics the impaired PTI responses observed in *ago1* mutants

(A) Detection of H_2O_2 production in the leaves of WT plants 24 hours after infiltration with the EtHAn strain alone (EtHAn) or with EtHAn strains carrying a plasmid encoding HopT1-1 or HopT1-1m3, respectively (left panel). Leaves from three plants were treated with ethanol to clear the chlorophyll pigments and were further incubated with DAB staining buffer to detect the presence of H_2O_2. Around 20-30

pictures were taken for each condition and absolute value of DAB staining was quantified using ImageJ software and presented as a dot plot (right panel). **(B)** Presence of callose deposits was detected 7 hours after infiltration of WT plants with the EtHAn strains used in (A). For each condition, leaves from three plants were collected and stained with aniline blue to detect the presence of callose deposits. The amount of callose deposits was measured using ImageJ software and presented as a dot plot. **(C)** Flg22-induced ROS production assay was performed in leaf discs from WT and *ago1* mutant alleles, *ago1-25, ago1-26 and ago1-27*. For each condition, leaves from three five-week-old plants were used to prepare leaf discs. Luminescence (Relative Light Unit; RLU) was subsequently measured for 45 min after flg22-elicitation for each technical replicate. Each dot represents the total amount of RLU produced during the flg22-elicitated time-course and the mean is represented as horizontal bar in the dot plot. **(D)** As in (C) but in WT, *ago1-27*, *dcl1-11* and *se-1* mutants. **(E)** Same analysis as in (A) but in WT *versus ago1-27* mutant plants infiltrated with Mock or EtHAn. **(F)** Same analysis as in (B) but in EtHAn-infiltrated WT plants versus *ago1-27* mutant. For all the above experiments, except for (E) and (F), statistical significance was assessed using one-way ANOVA analysis (*: p-value < 0.05; ****: p-value < 0.0001). For (E) and (F) experiments, statistical significance was assessed using student t-test (**: p-value < 0.01; ***: p-value < 0.001; ****: p-value < 0.0001). All the results shown in the different panels of the figure were obtained in at least two or three independent experiments represented in the dot plots as Rep1, Rep2 and Rep3, respectively.

Figure 6. Hypothetical model for HopT1-1-triggered suppression of PTI

In the absence of HopT1-1: Pathogen-Associated Molecular Patterns (PAMPs) from *Pto* DC3000 are perceived by plant Pattern Recognition Receptors (PRRs), which trigger downstream signalling events. The induction of a subset of conserved miRNAs, which are loaded into AGO1, is part of such PPR-mediated immune response (Navarro *et al*., 2006, Navarro *et al*., 2008, Li *et al*., 2010). Among those PAMP-responsive miRNAs, some act as positive regulators of defense by targeting Negative Regulators of PTI (NRPs), thereby ensuring a proper activation of PTI responses, including ROS production and callose deposition. For example, the flg22-induced miRNA miR160 orchestrates PAMP-triggered callose deposition, presumably by directing the silencing of some Auxin-Response Factors (e.g. *ARF17*) during PTI (Li *et al.,* 2010). In the presence of HopT1-1: the injected *Pto* DC3000 effector HopT1-1 physically interacts with AGO1 through, at least in part, two conserved GW motifs. This phenomenon alleviates miRNA-directed silencing of NRPs, resulting in their enhanced production. The increased accumulation of NRP proteins (e.g. ARF17) culminates in the dampening of PTI responses, including PAMP-triggered ROS production and callose deposition. FLS2, NRP, PTI and ROS stand for: Flagellin Sensing 2, Negative Regulator of PTI, PAMP-Triggered Immunity and Reactive Oxygen Species, respectively.

ACKNOWLEDGMENTS

We thank J. Chang for the EtHAn strain, O. Voinnet for DCL1, AGO2 and AGO4 antibodies, P. Genschik for the CFP-AGO1 construct and members of the Navarro Lab for critical reading of the manuscript. We are grateful to the PlantAlgae Facility of IBENS, which received support from the program “Investissements d’Avenir” ANR-10-Labx-54 MEMOLIFE and ANR-11-IDEX-0001-02 PSL* Research University and

of the SESAME Program from the “Région Île-de-France”; the Imaging Facility of IBENS, which received the support of grants from the “Région Île-de-France” (NERF N°2011-45), the “Fondation pour la Recherche Médicale” (N° DGE 20111123023) and the “Fédération pour la Recherche sur le Cerveau - Rotary International France” (2011), and the TRI-Genotoul platform, which was supported by the “Région Occitanie/Pyrénées-Méditerranée” (PRISM-Project). This work was supported by an European Research Council starting grant entitled “Silencing & Immunity” (to L.N.), an ATIP-Avenir Grant from the Fondation Bettencourt Schueller (to L.N.), a grant from the National Institutes of Health (to J.R.A.), and support from the Center for Plant Science Innovation at the University of Nebraska (to J.R.A.), by an ANR grant (08-BLAN-0206) and support from the CNRS (to T.L. and D.P.), by an ANR grant (15-CE20-0016-01) and support from the French Laboratory of Excellence ‘TULIP’ (ANR-10-LABX-41; ANR-11-IDEX-0002-02) (to L.D.) and by the “Région Occitanie/Pyrénées-Méditerranée” PRISM-Project (to C.P.).

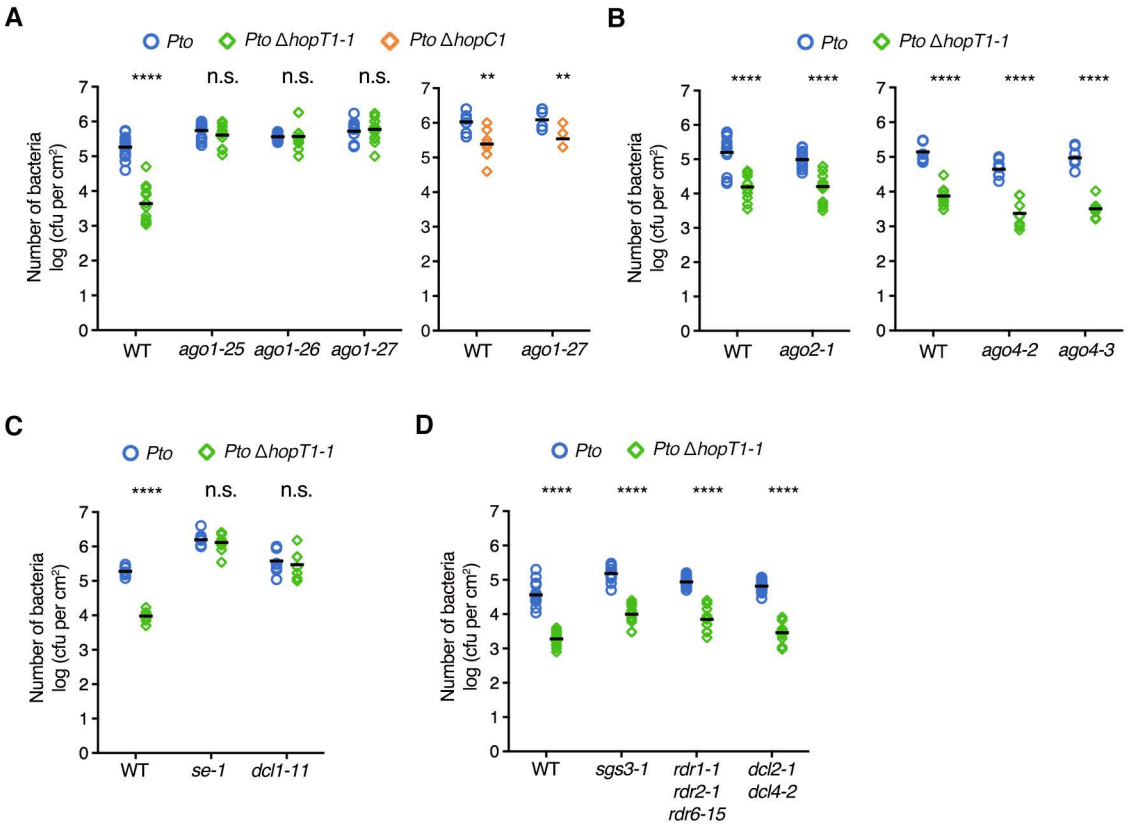

Figure 1. The growth defect of the hopT1-1-deleted strain of *Pto* DC3000 is specifically rescued in Arabidopsis miRNA-defective mutants
Five-week-old Col-0 Arabidopsis (WT) plants and indicated genotypes were dip- inoculated with bacterial strain *Pto* DC3000 (*Pto*) (blue dots) and *Pto* Δ hopT1-1 (green dots) or *Pto* ΔhopC1 (orange dots) at a concentration of 10^8 cfu/mL. At three days post-inoculation (3 dpi), leaves from three plants were collected and bacterial titers were further monitored. Each dot represents a number of bacteria as log (cfu per cm^2) and mean (n=8 or 16) is represented as horizontal line. Similar results were obtained in two to three independent experiments and are provided in Figure S1. **(A)** Left panel: growth of wild type *Pto* DC3000 strain (*Pto*) and of hopT1-1 deleted bacterial strain (*Pto* ΔhopT1-1) in WT plants and in three different hypomorphic *ago1* mutants, namely *ago1-25*, *ago1-26* and *ago1-27*. Right panel: growth of wild type *Pto* DC3000 strain (*Pto*) and of hopC1 deleted bacterial strain (*Pto* ΔhopC1) in WT plants and in *ago1-27* mutant. **(B)** Growth of WT *Pto* and of *Pto* ΔhopT1-1 in WT plants and in mutants defective in AGO2 (*ago2-1*) or in AGO4 (*ago4-2* and *ago4-3*). **(C)** Same as in (A-Left panel) but in miRNA biogenesis-defective mutants *se-1* and *dcl1-11*. **(D)** Same as in (B) but in siRNA biogenesis mutants: *sgs3-1*, *rdr1-1 rdr2-1 rdr6-15* and *dcl2-1 dcl4-2*. Statistical significance was assessed using the ANOVA test (n.s.: p-value > 0.05; *: p-value < 0.05; **: p-value < 0.01; ***: p-value < 0.001; ****: p-value < 0.0001).

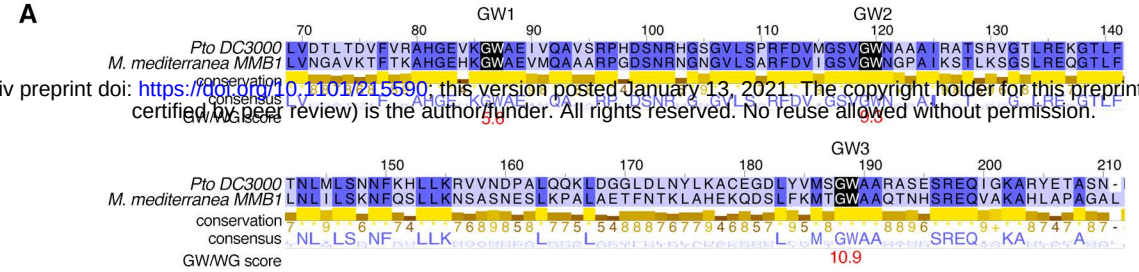

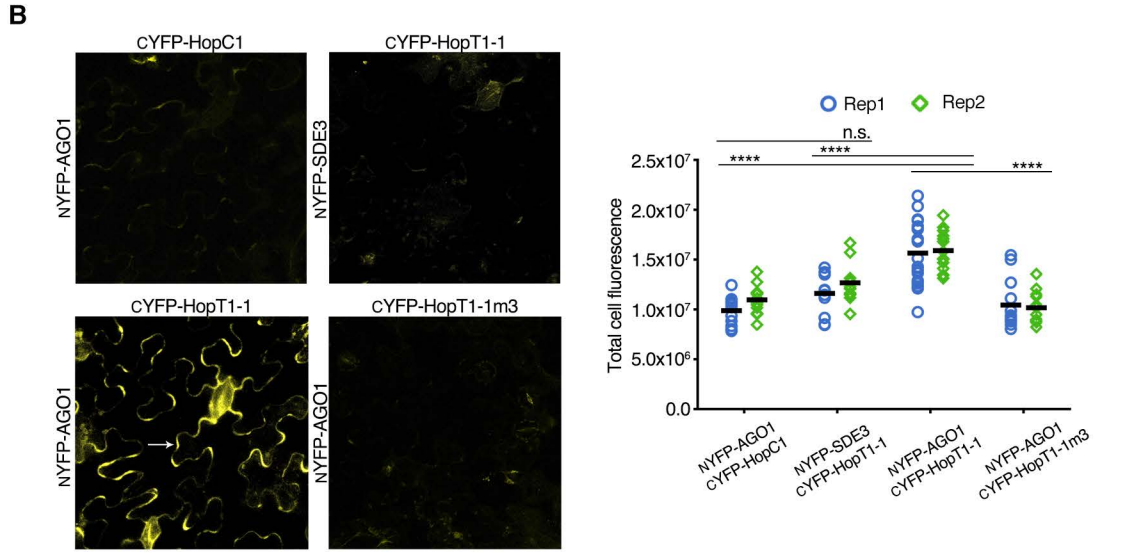

C

Donor	Acceptor	τ	sem[a]	Δ[b]	N[c]	E[d]	p-value
CFP-AGO1	-	2.858	0.029	-	79	-	-
CFP-AGO1	HopT1-1-YFP	2.516	0.032	342	60	11.2	$2E^{-10}$
CFP-AGO1	HopT1-m3-YFP	2.904	0.034	46	50	1.61	0.32
CFP-AGO1	HopT1-1-HA	2.8	0.028	28	34	0.99	0.65

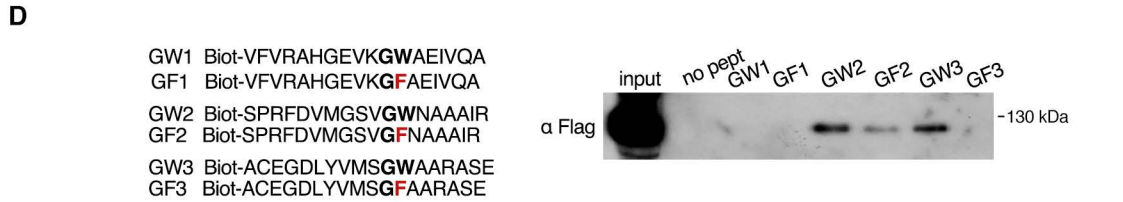

Figure 2. HopT1-1 possesses two conserved GW motifs that are required for HopT1-1-AGO1 interaction

(A) Partial sequences (69-210 amino acids) of the *Pto* DC3000 HopT1-1 (NP_808678.1) and the *Marinomonas mediterranea* MMB-1 HopT1-1 (WP_013659626.1) proteins were aligned using clustalW2. These protein sequences possess three conserved GW motifs (named GW1, GW2 and GW3) highlighted in black boxes. The score of GW motifs prediction was retrieved by using the matrix AGO-planVir of the web portal http://150.254.123.165/whub/ (Zielezinski and Karlowsk, 2015) and is indicated below each GW motif. **(B)** BiFC assay in *N. benthamiana*. Four-week-old *N. benthamiana* were co-infiltrated with combinations of *Agrobacterium tumefaciens* strains carrying different constructs fused with N-terminal or C-terminal part of YFP. Interaction of NYFP-AGO1 with CYFP-HopT1-1 (left bottom) or with CYFP-HopT1-1m3 (right bottom) was tested. As negative controls, NYFP-AGO1 was co-infiltrated with CYFP-HopC1 (left top) and NYFP-SDE3 was co-infiltrated with CYFP-HopT1-1 (right top). YFP fluorescence was visualized by confocal microscopy three days post-infiltration (left panel) and quantification of the fluorescence signal for each picture taken (n=10) was performed using ImageJ software (right panel). Each dot represents the intensity of fluorescence signal in epidermal cells (white arrow) resulting from the interaction of each pair of combination as indicated in the dot plot. The signal in stomata cells is likely due to autofluorescence and should thus not be considered as positive BiFC signal. Two biological replicates are presented and the mean is represented as the horizontal line. Statistical significance was assessed using the ANOVA test (n.s.: p-value > 0.05; ****: p-value < 0.0001). **(C)** FRET-FLIM measurements showing that HopT1-1, but not HopT1-1m3, interacts with AGO1 in the cytoplasm of plant cells. Mean lifetime, $_{\tau}$, is in nanoseconds (ns). [a] For each cell analyzed, average fluorescence decay profiles measured in the cytoplasm were plotted and fitted with exponential function using a non-linear square estimation procedure, and the mean lifetime was calculated according to to $\tau = \sum \langle_i \tau_i^2 / \sum \langle_i \tau_i$ with $I(t) = \sum \alpha_i e^{-t/\tau i}$, standard error of the mean, [b] $\Delta t = {}_{\tau D} - {}_{\tau DA}$ (in ps), [c] total number of measured cell cytoplasm, and [d] % FRET efficiency: $E = 1 - ({}_{\tau DA}/{}_{\tau D})$. p-value of the difference between the donor lifetimes in the presence and in the absence of acceptor (Student's *t* test). **(D)** To assess which GW motif/s of HopT1-1 is/are required for the interaction with AGO1, synthetic biotinylated peptides containing the WT (GW) or the mutated version (GF) of each GW motif of HopT1-1 were mobilized on streptavidin magnetic beads. Specific peptide-loaded beads were further incubated with total protein extracted from Flag-AGO1 inflorescence. The presence of Flag-AGO1 in the total protein extract (input) and bound to the beads was assessed by immunoblotting. The peptides GW2 and GW3, but not GW1, can interact with Flag-AGO1. This interaction was partially or completely impaired in presence of GF2 and GF3, respectively.

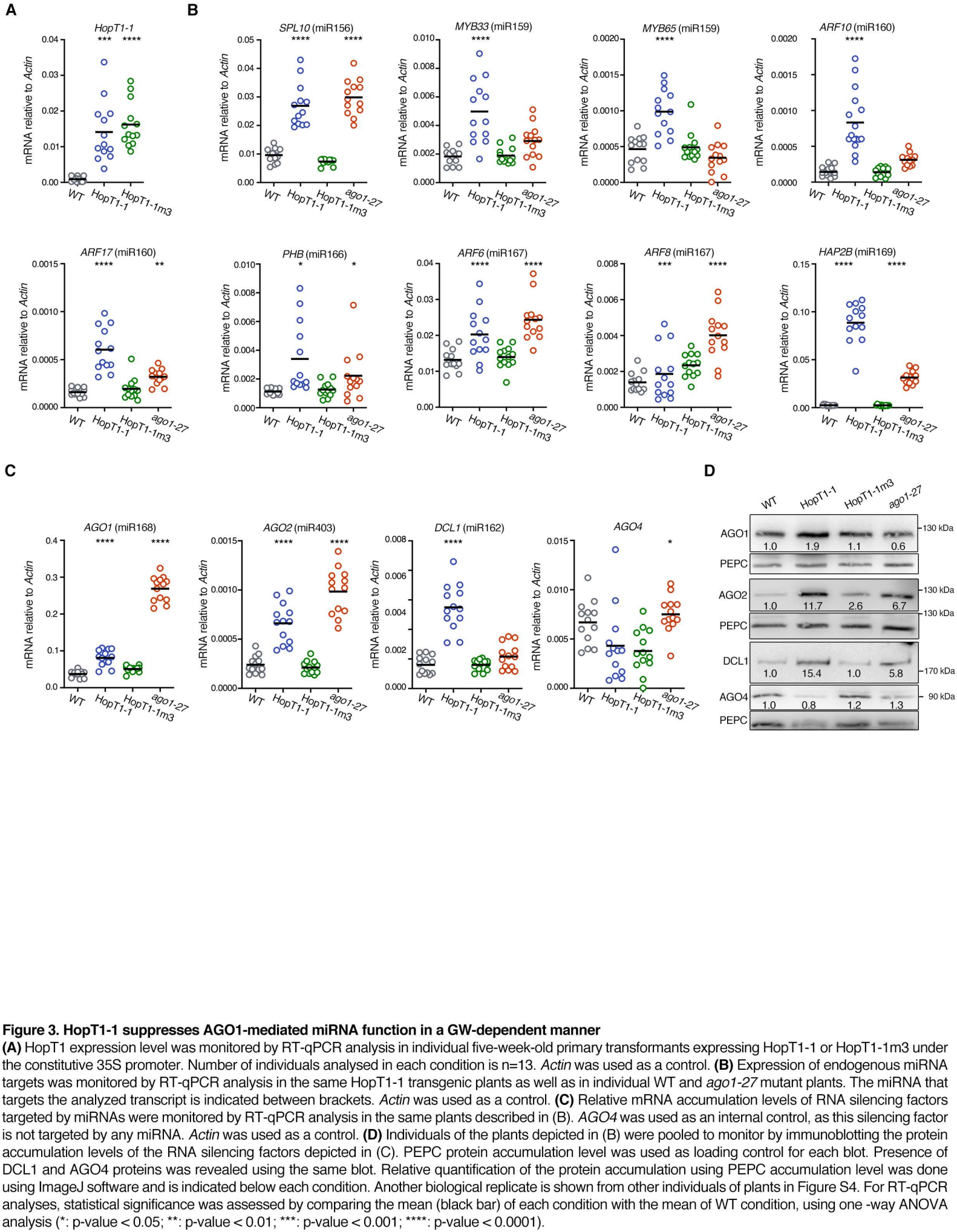

Figure 3. HopT1-1 suppresses AGO1-mediated miRNA function in a GW-dependent manner

(A) HopT1 expression level was monitored by RT-qPCR analysis in individual five-week-old primary transformants expressing HopT1-1 or HopT1-1m3 under the constitutive 35S promoter. Number of individuals analysed in each condition is n=13. *Actin* was used as a control. **(B)** Expression of endogenous miRNA targets was monitored by RT-qPCR analysis in the same HopT1-1 transgenic plants as well as in individual WT and *ago1-27* mutant plants. The miRNA that targets the analyzed transcript is indicated between brackets. *Actin* was used as a control. **(C)** Relative mRNA accumulation levels of RNA silencing factors targeted by miRNAs were monitored by RT-qPCR analysis in the same plants described in (B). *AGO4* was used as an internal control, as this silencing factor is not targeted by any miRNA. *Actin* was used as a control. **(D)** Individuals of the plants depicted in (B) were pooled to monitor by immunoblotting the protein accumulation levels of the RNA silencing factors depicted in (C). PEPC protein accumulation level was used as loading control for each blot. Presence of DCL1 and AGO4 proteins was revealed using the same blot. Relative quantification of the protein accumulation using PEPC accumulation level was done using ImageJ software and is indicated below each condition. Another biological replicate is shown from other individuals of plants in Figure S4. For RT-qPCR analyses, statistical significance was assessed by comparing the mean (black bar) of each condition with the mean of WT condition, using one -way ANOVA analysis (*: p-value < 0.05; **: p-value < 0.01; ***: p-value < 0.001; ****: p-value < 0.0001).

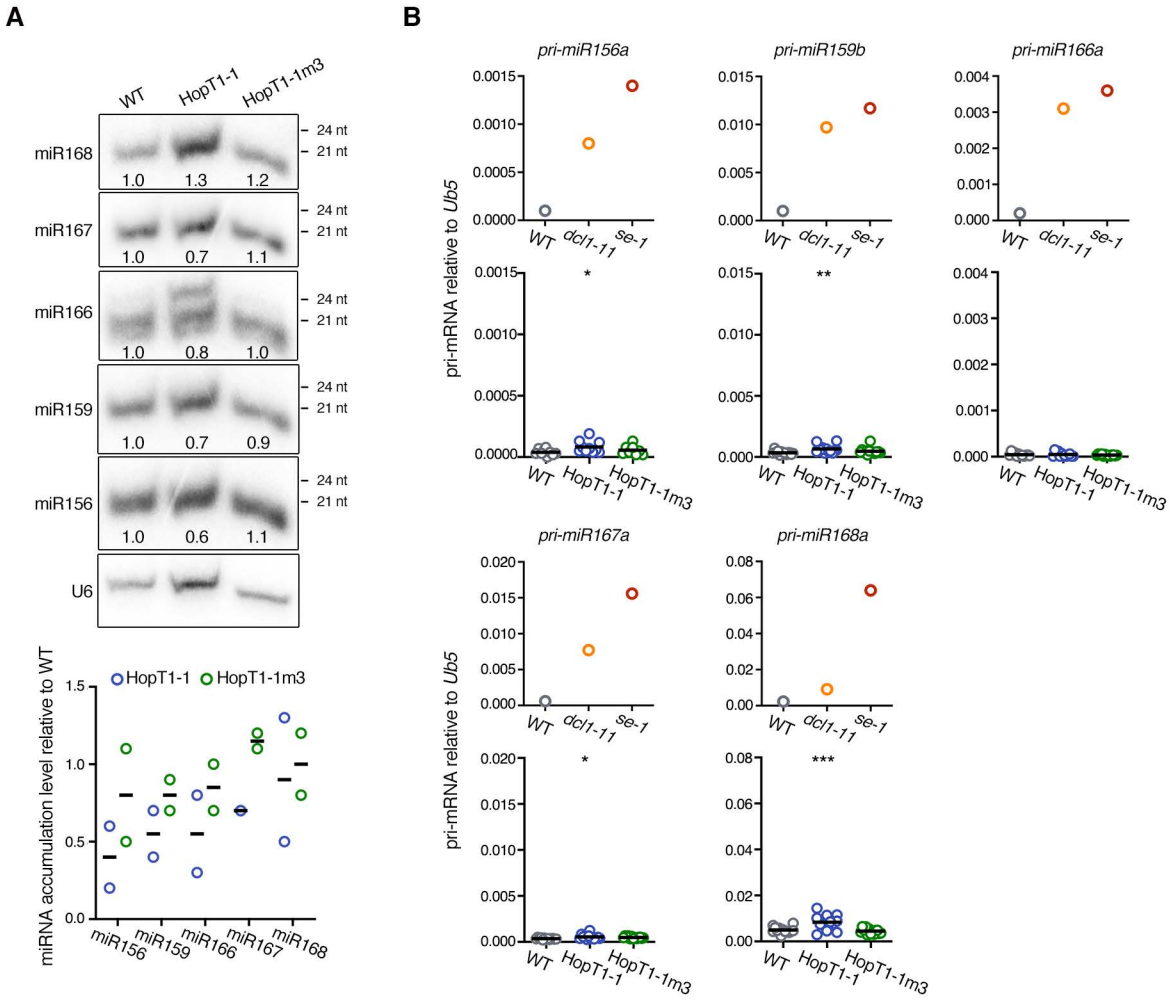

Figure 4. The AGO-binding platform of HopT1-1 triggers a moderate decrease in the accumulation of a subset of conserved miRNAs, while it does not, or negligibly, interfere with the processing of cognate pri-miRNAs.

(A) Top panels: Accumulation levels of endogenous miRNAs in pooled WT plants and in pooled primary transformants expressing HopT1-1 or HopT1-1m3 were assessed by northern blot. U6 was used as a loading control. Bottom panel: quantification of the miRNA accumulation level in HopT1-1 and in HopT1-1m3 plants relative to the miRNA accumulation in WT plants is shown for two biological replicates (Figures 4A and S5A). **(B)** Accumulation levels of endogenous pri-miRNAs were assessed by RT-qPCR in five-week-old WT plants and in *dcl1-11* and *se-1* mutants (top panels) or in the plants described in Figure 3A (bottom panels). *Ubiquitin5* (*ub5*) was used as a control. For the RT-qPCR analysis of HopT1-1 and HopT1-1m3 transgenic plants, statistical significance was assessed by comparing the mean (black bar) of each condition with the mean of WT condition, using one -way ANOVA analysis (*: p-value < 0.05;

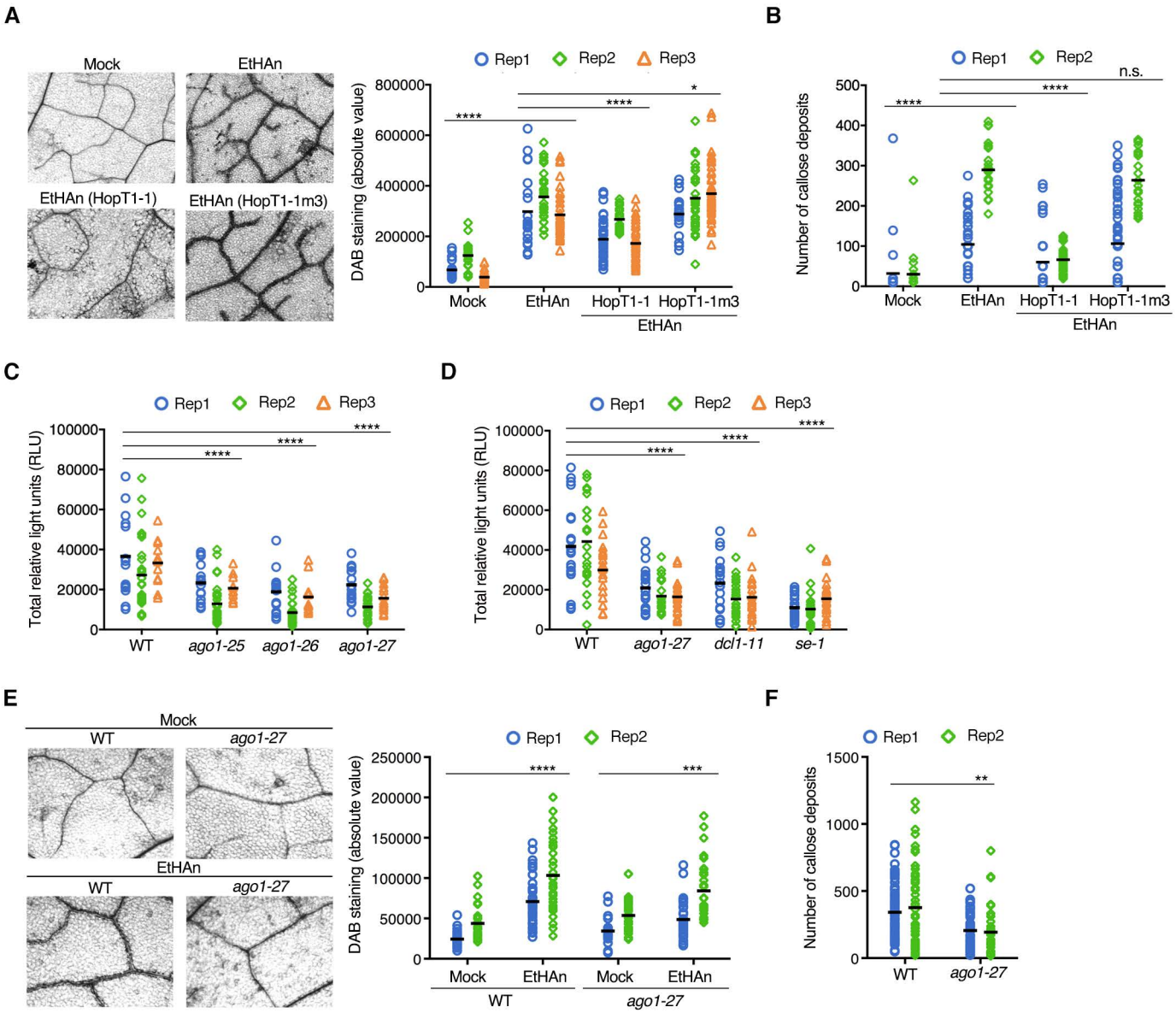

Figure 5. HopT1-1 dampens PTI in a GW-dependent manner and its presence mimics the impaired PTI responses observed in *ago1* mutants

(A) Detection of H_2O_2 production in the leaves of WT plants 24 hours after infiltration with the EtHAn strain alone (EtHAn) or with EtHAn strains carrying a plasmid encoding HopT1-1 or HopT1-1m3, respectively (left panel). Leaves from three plants were treated with ethanol to clear the chlorophyll pigments and were further incubated with DAB staining buffer to detect the presence of H_2O_2. Around 20-30 pictures were taken for each condition and absolute value of DAB staining was quantified using ImageJ software and presented as a dot plot (right panel). **(B)** Presence of callose deposits was detected 7 hours after infiltration of WT plants with the EtHAn strains used in (A). For each condition, leaves from three plants were collected and stained with aniline blue to detect the presence of callose deposits. The amount of callose deposits was measured using ImageJ software and presented as a dot plot. **(C)** Flg22-induced ROS production assay was performed in leaf discs from WT and *ago1* mutant alleles, *ago1-25*, *ago1-26* and *ago1-27*. For each condition, leaves from three five-week-old plants were used to prepare leaf discs. Luminescence (Relative Light Unit; RLU) was measured for 45 min after flg22-elicitation for each technical replicate. Each dot represents the total amount of RLU produced during the flg22-elicitated time-course and the mean is represented as horizontal bar in the dot plot. **(D)** As in (C) but in WT, *ago1-27*, *dcl1-11* and *se-1* mutants. **(E)** Same analysis as in (A) but in WT versus *ago1-27* mutant plants infiltrated with Mock or EtHAn. **(F)** Same analysis as in (B) but in EtHAn-infiltrated WT plants versus *ago1-27* mutant. For all the above experiments, except for (E) and (F), statistical significance was assessed using one-way ANOVA analysis (*: p-value < 0.05; ****: p-value < s0.0001). For (E) and (F) experiments, statistical significance was assessed using student t-test (**: p-value < 0.01; ***: p-value < 0.001; ****: p-value < 0.0001). All the results shown in different panels of the figure were obtained in at least two or three independent experiments represented in the dot plots as Rep1, Rep2 and Rep3, respectively.

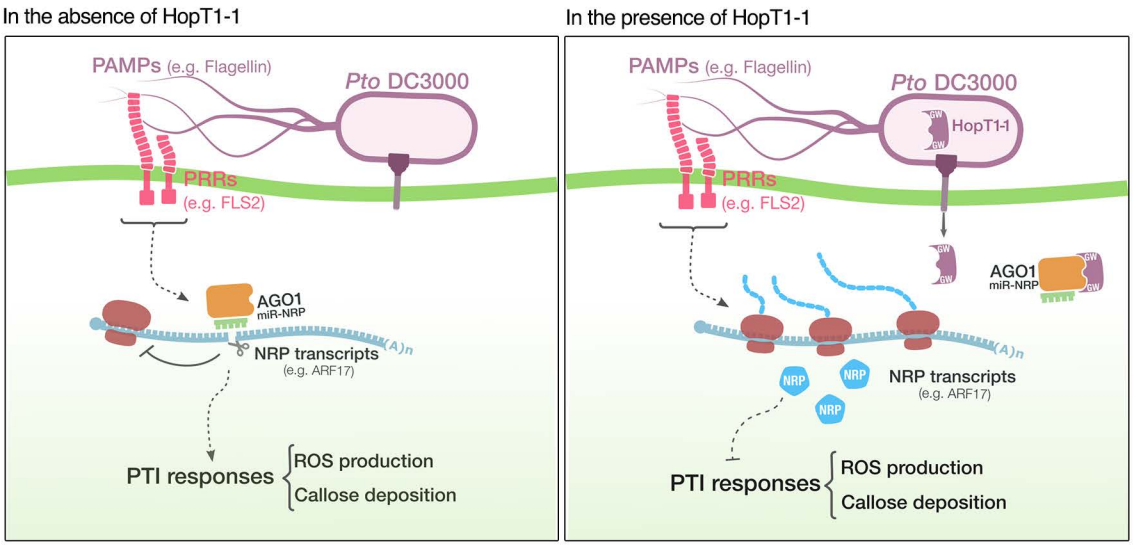

Figure 6. Hypothetical model for HopT1-1-triggered suppression of PTI

In the absence of HopT1-1: Pathogen-Associated Molecular Patterns (PAMPs) from *Pto* DC3000 are perceived by plant Pattern Recognition Receptors (PRRs), which trigger downstream signalling events. The induction of a subset of conserved miRNAs, which are loaded into AGO1, is part of such PPR-mediated immune response (Navarro *et al.*, 2006, Navarro *et al.*, 2008, Li *et al.*, 2010). Among those PAMP-responsive miRNAs, some act as positive regulators of defense by targeting Negative Regulators of PTI (NRPs), thereby ensuring a proper activation of PTI responses, including ROS production and callose deposition. For example, the flg22-induced miRNA miR160 orchestrates PAMP-triggered callose deposition, presumably by directing the silencing of some Auxin-Response Factors (e.g. ARF17) during PTI (Li *et al.*, 2010). In the presence of HopT1-1: the injected Pto DC3000 effector HopT1-1 physically interacts with AGO1 through, at least in part, two conserved GW motifs. This phenomenon alleviates miRNA-directed silencing of NRPs, resulting in their enhanced production. The increased accumulation of NRP proteins (e.g. ARF17) culminates in the dampening of PTI responses, including PAMP-triggered ROS production and callose deposition. FLS2, NRP, PTI and ROS stand for: Flagellin Sensing 2, Negative Regulator of PTI, PAMP-Triggered Immunity and Reactive Oxygen Species, respectively.